Correlating electroluminescence characterization and physics-based models of InGaN/GaN LEDs: Pitfalls and open issues

Cite as: AIP Advances **4**, 067118 (2014); https://doi.org/10.1063/1.4882176
Submitted: 05 December 2013 . Accepted: 28 May 2014 . Published Online: 05 June 2014

Marco Calciati, Michele Goano, Francesco Bertazzi, Marco Vallone, Xiangyu Zhou, Giovanni Ghione, Matteo Meneghini, Gaudenzio Meneghesso, Enrico Zanoni, Enrico Bellotti, Giovanni Verzellesi, Dandan Zhu, and Colin Humphreys

Correlating electroluminescence characterization and physics-based models of InGaN/GaN LEDs: Pitfalls and open issues

Marco Calciati,[1] Michele Goano,[1,2,a] Francesco Bertazzi,[1,2] Marco Vallone,[1] Xiangyu Zhou,[1] Giovanni Ghione,[1] Matteo Meneghini,[3] Gaudenzio Meneghesso,[3] Enrico Zanoni,[3] Enrico Bellotti,[4] Giovanni Verzellesi,[5] Dandan Zhu,[6] and Colin Humphreys[6]

[1]*Dipartimento di Elettronica e Telecomunicazioni, Politecnico di Torino, corso Duca degli Abruzzi 24, 10129 Torino, Italy*

[2]*IEIIT-CNR, Politecnico di Torino, corso Duca degli Abruzzi 24, 10129 Torino, Italy*

[3]*Dipartimento di Ingegneria dell'Informazione, Università di Padova, Via Gradenigo 6/B, 35131 Padova, Italy*

[4]*Department of Electrical and Computer Engineering, Boston University, 8 Saint Mary's Street, 02215 Boston, MA, USA*

[5]*Dipartimento di Scienze e Metodi dell'Ingegneria, Università di Modena e Reggio Emilia, 42122 Reggio Emilia, Italy*

[6]*Department of Materials Science and Metallurgy, University of Cambridge, 27 Charles Babbage Road, Cambridge CB3 0FS, United Kingdom*

(Received 5 December 2013; accepted 28 May 2014; published online 5 June 2014)

Electroluminescence (EL) characterization of InGaN/GaN light-emitting diodes (LEDs), coupled with numerical device models of different sophistication, is routinely adopted not only to establish correlations between device efficiency and structural features, but also to make inferences about the loss mechanisms responsible for LED efficiency droop at high driving currents. The limits of this investigative approach are discussed here in a case study based on a comprehensive set of current- and temperature-dependent EL data from blue LEDs with low and high densities of threading dislocations (TDs). First, the effects limiting the applicability of simpler (closed-form and/or one-dimensional) classes of models are addressed, like lateral current crowding, vertical carrier distribution nonuniformity, and interband transition broadening. Then, the major sources of uncertainty affecting state-of-the-art numerical device simulation are reviewed and discussed, including (i) the approximations in the transport description through the multi-quantum-well active region, (ii) the alternative valence band parametrizations proposed to calculate the spontaneous emission rate, (iii) the difficulties in defining the Auger coefficients due to inadequacies in the microscopic quantum well description and the possible presence of extra, non-Auger high-current-density recombination mechanisms and/or Auger-induced leakage. In the case of the present LED structures, the application of three-dimensional numerical-simulation-based analysis to the EL data leads to an explanation of efficiency droop in terms of TD-related and Auger-like nonradiative losses, with a C coefficient in the 10^{-30} cm^6/s range at room temperature, close to the larger theoretical calculations reported so far. However, a study of the combined effects of structural and model uncertainties suggests that the C values thus determined could be overestimated by about an order of magnitude. This preliminary attempt at uncertainty quantification confirms, beyond the present case, the need for an improved description of carrier transport and microscopic radiative and nonradiative recombination mechanisms in device-level LED

[a]Electronic mail: michele.goano@polito.it

[http://dx.doi.org/10.1063/1.4882176]

I. INTRODUCTION

The ongoing debate on efficiency droop in GaN-based light-emitting diodes (LEDs)[1–6] attests the present limitations of both characterization techniques and numerical models of III-nitride active optoelectronic devices. The inadequacies of the standard drift-diffusion (DD) simulation framework when used to describe carrier transport across a LED active region[7,8] have elicited the inclusion of semiempirical corrections for mechanisms such as tunneling,[9,10] carrier overflow,[11,12] ballistic overshoot,[13–15] "nonlocal" transport between quantum wells (QWs),[16] and Auger-induced leakage.[17] Unfortunately, the effects of those mechanisms are often hard to discriminate experimentally, which results in a problematic validation of the corresponding models. These intrinsic difficulties are compounded by at least three factors:

a. the enduring lack of reliable first-principles models for nonradiative and radiative recombination mechanisms and other critical physical parameters (band offsets at heterojunctions,[18,19] interface polarization charges,[20,21] etc.) in realistic InGaN QWs,
b. the inconsistencies in the definitions of some optical and transport parameters when used in experimental and in simulation contexts (e.g., "bulk" Auger coefficients vs. Auger rates in two-dimensional systems[22]),
c. the large (but often unacknowledged) sensitivity of several key parameters to technological/structural details (interface quality, layer homogeneity, doping and composition profiles, etc.) often unaccessible to an accurate experimental determination,

to which one could add the bias towards simpler, single-mechanism explanations against more comprehensive descriptions.[23–25]

We set out to illustrate the main issues faced when performing a combined experimental and simulation-based analysis of InGaN/GaN blue LEDs with an example carried out on a set of devices grown, characterized and simulated by the authors. Section II describes the test devices and presents the results of a systematic electroluminescence (EL) characterization for different temperatures, essential in the determination of the relative importance of competing loss mechanisms.[26] After several critical structure-related issues are addressed in Section III (contact geometry, interplay between current crowding, current leakage and vertical nonuniformity of carrier densities, etc.), Section IV applies two- and three-dimensional (2D, 3D) numerical device simulation to the determination of "optimal" recombination parameters allowing to reproduce the experimental *L*/*I* ratio as a function of current density and temperature. The results of this study, leading to an explanation of efficiency droop in terms of Auger-like nonradiative losses characterized by a *C* coefficient in the 10^{-30} cm^6/s range at room temperature, are critically discussed in Section V, where the uncertainties and limitations of the modeling framework are shown to correspond to a possible *C* overestimation by about an order of magnitude and, more generally, underscore the problematic identification between the Auger-like *C* coefficient considered by DD analysis and the actual Auger rates. As a conclusion, Section VI makes briefly the case for an improved microscopic model based on a more realistic description of the dynamics and distribution functions of carriers.

II. STRUCTURE AND EXPERIMENTS

In order to help discriminate the recombination coefficients, our study was carried out on two sets of nominally identical LED structures grown on GaN templates differing for their threading dislocation densities (TDDs) N_{disl}. Low TDD (LDD) samples have $N_{\mathrm{disl}} \approx 3 \times 10^8$ cm^{-2}, while high TDD (HDD) devices have $N_{\mathrm{disl}} \approx 8 \times 10^9$ cm^{-2}. On top of the substrate, having a 100 μm nominal thickness, is a 2.6 μm-thick GaN buffer layer, with a *n*-type doping density $4 \cdot 10^{18}$ cm^{-3}.

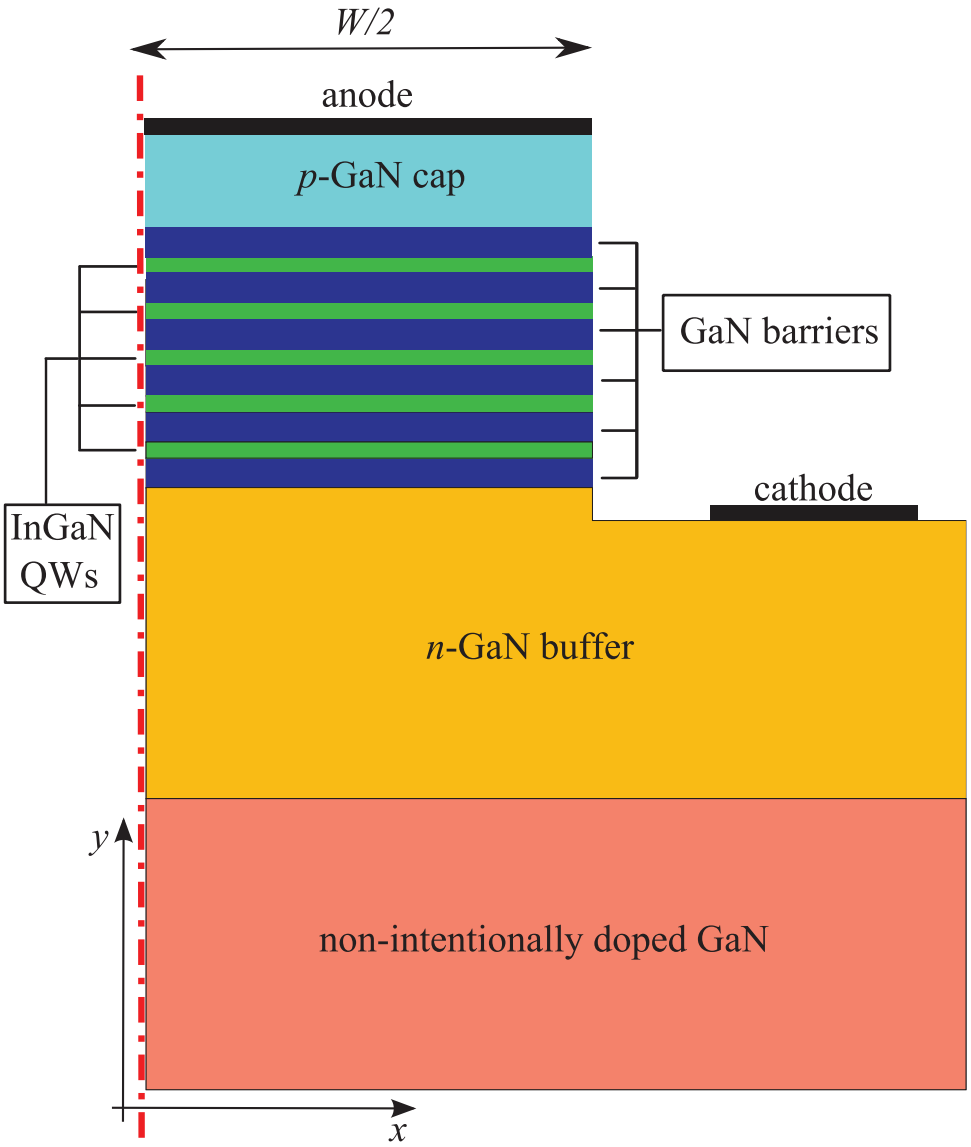

FIG. 1. Schematic cross-section of the LEDs under study. Only one half of the structure is reported, thanks to the symmetry along the lateral direction (x). The symmetry axis at the center of the mesa is represented as a dashed line. The figure is not drawn to scale, since the aspect ratio W/H of the mesa is larger than 10^3.

The active region, designed for 470 nm emission wavelength and non-intentionally-doped, has a total thickness of 64 nm and includes five InGaN QWs separated by GaN quantum barriers (QBs), with no electron or hole blocking layer (EBL/HBL). The absence of an EBL seems to have little impact on the onset of droop in the devices under study; a discussion is presented in Section III. The epitaxial stack is completed by a 130 nm-thick GaN cap layer with p-type doping level $3 \cdot 10^{19}$ cm^{-3}. From high resolution x-ray diffraction (HRXRD) spectra, the combined thickness of a QW/QB pair has been determined as 11.5 nm in both the LDD and HDD structures, while the In molar fraction in the QWs is in the range 0.15–0.20. As a limiting case, all simulations presented in Sections III and IV will assume in the active region an ideally piecewise constant composition profile with undoped 5 nm-thick $In_{0.15}Ga_{0.85}N$ QWs and 6.5 nm-thick GaN QBs; the effects of deviations from these values will be briefly discussed in Section V C.

Through an etching process, the LEDs are patterned into square mesas, having width $W = 0.5$ mm and total nominal height $H = 320$ nm (about 130 nm of the n-type buffer have been

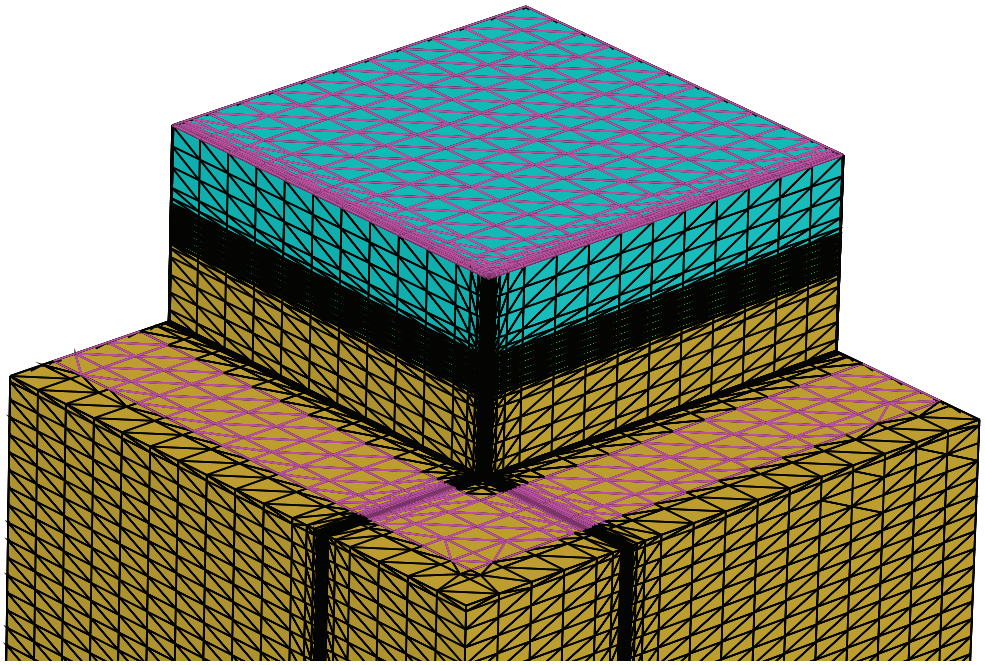

FIG. 2. Mesh used in the 3D simulations of the LEDs under study. Thanks to the structural symmetries in the (x, y) plane, only one fourth of the entire device has been discretized, so that the topmost corner in the figure corresponds to the mesa center. The anode contact (covering the top surface of the mesa) and the cathode contact (a square ring deposited on the etched GaN buffer) are shown in purple. In order to better identify the active region, the vertical axis in the plot has been expanded by a factor 300.

etched). The p-type top layer is completely covered with a uniform, non-roughened semitransparent square contact of area $S = W^2 = 0.25$ mm^2. Finally, a 60 μm-wide cathode contact metallization is deposited on the partially exposed n-type GaN buffer, surrounding the entire mesa periphery at a 20 μm distance from the mesa sidewalls. A schematic cross-section of the LEDs under study and a detail of the mesh used in the 3D simulations are shown in Figs. 1 and 2.

The $I(V)$ and $L(I)$ characteristics (where V is the applied voltage, I is the current flowing through the anode and cathode contacts, $L = \eta_{\text{extr}} P_{\text{op}}$ is the emitted optical power, P_{op} is the total optical power generated in the active region, η_{extr} is the extraction efficiency) and the EL spectra were measured under pulsed excitation over a controlled temperature range between 15 °C and 120 °C. In Fig. 3 are shown the experimental EL spectra for different temperatures in the LDD and HDD LEDs, respectively. Experimental results indicate that, predictably, LDD LEDs exhibit a significantly higher efficiency: the peak L/I ratio at room temperature in LDD LEDs is about twice as large as in HDD ones, see Fig. 4. LDD devices are also affected by a much smaller temperature sensitivity of the quantum efficiency; for an injection current $I = 100$ mA, corresponding to a current density $J = 40$ A/cm^2, a temperature increase $\Delta T = 105$ °C leads to a reduction in the emitted optical power equal to 50% and just 10% in HDD and LDD LEDs, respectively (see Fig. 5). LDD LEDs show also a significant improvement in the stability of the peak emission wavelength λ_{peak} with respect to both temperature and injection current (see Fig. 6).

III. PRELIMINARY MODELING CONSIDERATIONS

Our simulation analysis has been based on the APSYS modeling software from Crosslight Software Inc. and, to a lesser extent, on the TCAD SENTAURUS suite from Synopsys Inc. APSYS and TCAD SENTAURUS ARE WELL REPRESENTATIVE OF THE STATE OF THE ART IN OPTOELECTRONIC COMPUTER-AIDED DESIGN (CAD) TOOLS, WHOSE LIMITATIONS ARE THE FOCUS OF OUR INVESTIGATION. BOTH implement 2D and 3D DD models coupled with relevant quantum corrections, including the self-consistent solution of Poisson and Schrödinger equations in the active region. The

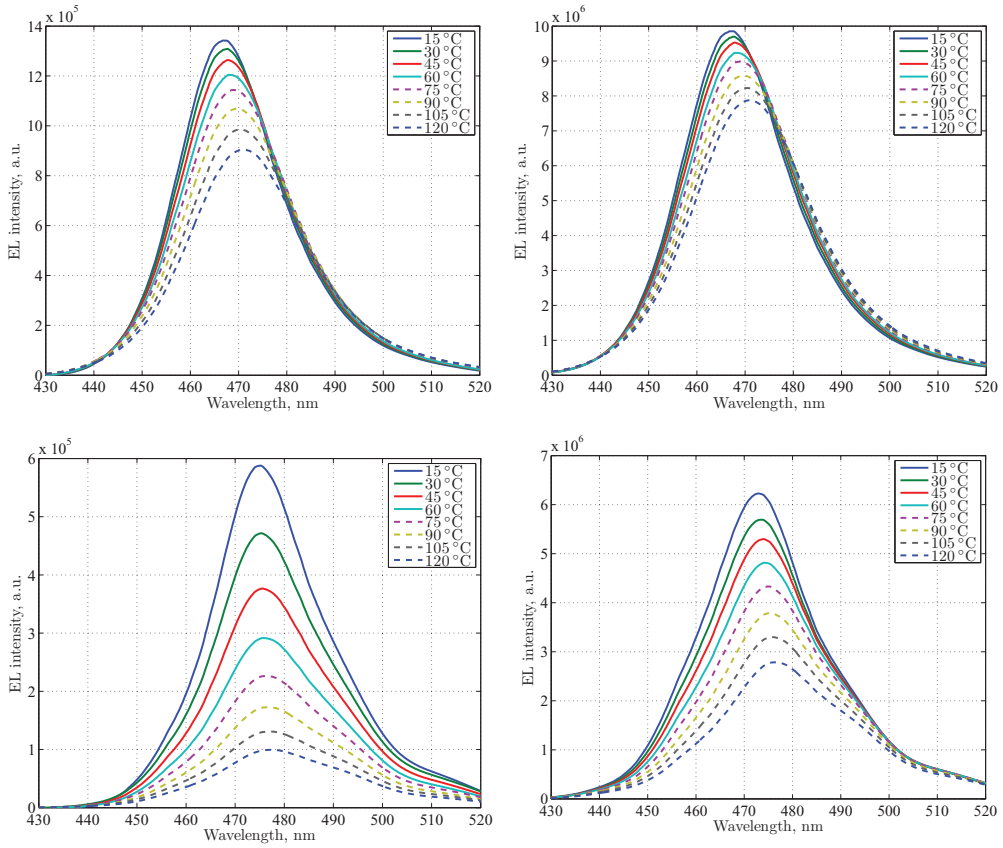

FIG. 3. Experimental EL spectra for different temperatures in a LDD (top) and HDD (bottom) LED. $I = 10$ mA, $J = 4$ A/cm^2 (left), $I = 100$ mA, $J = 40$ A/cm^2 (right).

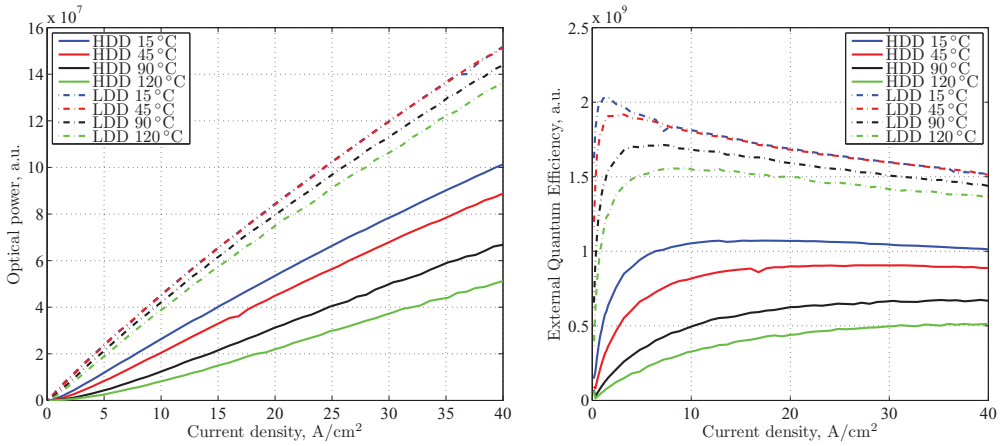

FIG. 4. Measured emitted optical power (left) and corresponding experimental ratio *L*/*I* (right) as functions of the injection current density at different temperatures in a LDD (dashed lines) and HDD (solid lines) LED.

valence band is described with a $\boldsymbol{k} \cdot \boldsymbol{p}$ Hamiltonian, allowing the determination of spontaneous emission as a function of wavelength and carrier density in strained QWs; many-body effects are also accounted for. Specific features of non-cubic semiconductors are taken into account, such as the spontaneous and piezoelectric polarization effects, and the description of carrier transport across the active region may be corrected with semiempirical models for e.g. tunneling and capture/escape

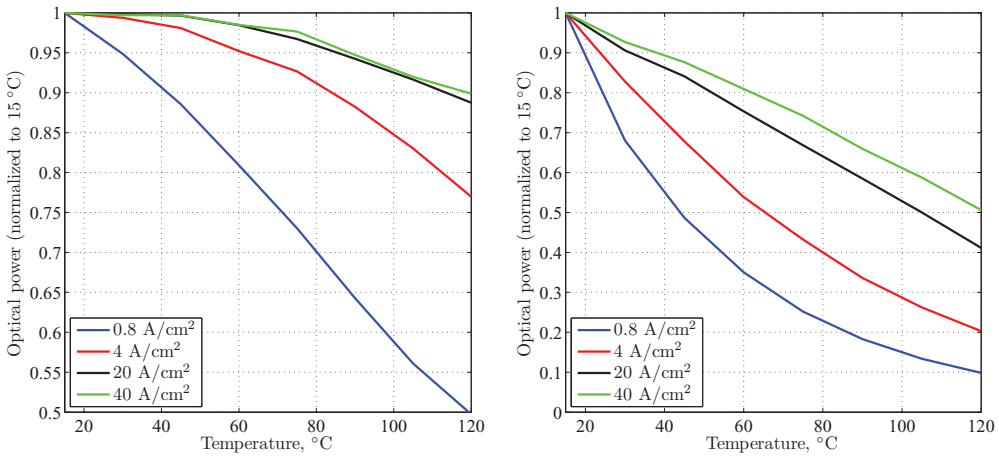

FIG. 5. Measured emitted optical power as a function of temperature at different injection current densities in a LDD (left) and HDD (right) LED. Each curve has been normalized with respect to its value at $T = 15\,^{\circ}\mathrm{C}$.

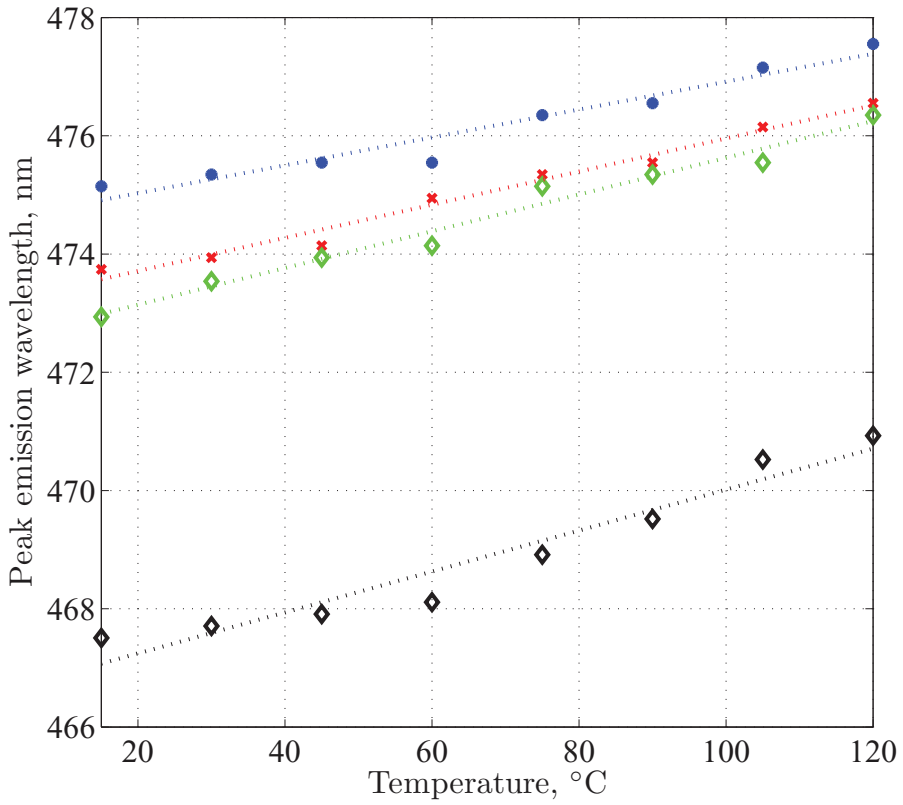

FIG. 6. Measured λ_{peak} as a function of temperature in a LDD LED (black symbols, independent of the injection current density) and a HDD LED (blue: $J = 4$ A/cm^2; red: 20 A/cm^2; green: 40 A/cm^2).

processes between QWs and barriers. The nominal values of the material parameters used in the present simulations are reported in Appendix A 1.

Before addressing, in Section IV, the use of 3D simulation to extract "optimal" recombination coefficients allowing to reproduce the experimental *L*/*I* ratios as functions of current density, temperature and TDD, some preliminary considerations on our test devices are in order, relevant also to most LEDs discussed in the literature.

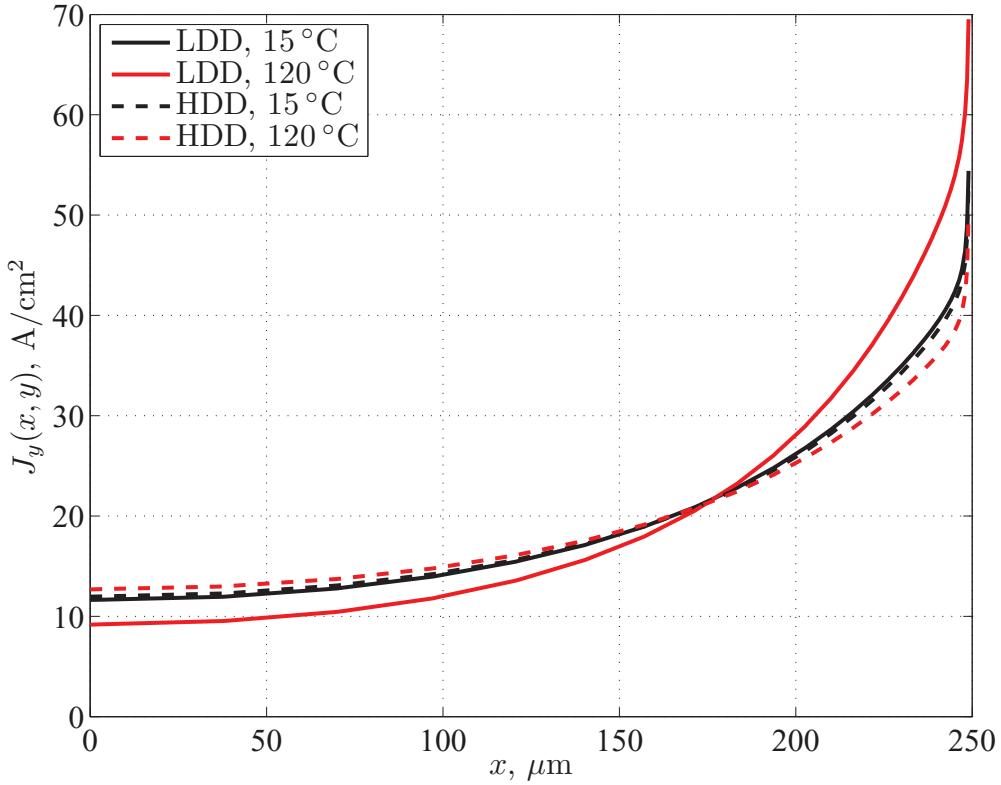

FIG. 7. Simulated vertical component of the total current density J_y as a function of the lateral coordinate x (measured from the center of the 0.5 mm-wide mesa), across a horizontal section located 100 nm below the bottom barrier of the active region, at an injection current $I = 100$ mA ($J = 40$ A/cm^2). The current profiles $J_y(x)$ in a LDD (solid lines) and HDD (dashed lines) LED at $T = 15\,^\circ$C (black lines) and $T = 120\,^\circ$C (red lines) are compared.

A. Realistic spatial distribution of carriers in the active region

The standard *ABC* model used for correlating current and carrier density in the analysis of experimental data is:[27]

$$I = qV_{\mathrm{QW}}(An + Bn^2 + Cn^3) + I_{\mathrm{leak}} \tag{1}$$

where A, B, C are the "effective" Shockley-Read-Hall (SRH), radiative, and Auger recombination coefficients in the QWs, q is the electron charge, V_{QW} is the volume of all QWs, and I_{leak} accounts for all other loss mechanisms. This model is based on two main implicit assumptions about electron and hole densities $n(x, y)$, $p(x, y)$ in the QWs comprised into the active region: both n and p are essentially constant along x and y, and $n \approx p$. These conditions should be satisfied also when more detailed models for the *ABC* coefficients are used, e.g. when their possible saturation at high carrier densities is taken into account[27,28] (as a general rule, the Auger recombination rate is proportional to n^3 only if the Maxwell-Boltzmann carrier statistics can be used, but this is not usually the case in LEDs and lasers) or density-activated defect recombination (DADR) is considered.[29] Moreover, all leakage mechanisms, including carrier overflow (thermionic emission),[11,12] non-capture by the QWs or ballistic overshoot,[13–15] tunneling,[9,10] and Auger-induced leakage[17] are usually either neglected or empirically approximated with n-dependent models. Some groups have also proposed *ABCD* models to describe leakage, and numerical estimates of a third (or higher) order coefficient corresponding to its effects have been presented e.g. in Refs. 30–33.

Contrary to the one-dimensional (1D) charge-control models based on Eq. (1), a 3D DD simulation framework can take into account selfconsistently carrier nonuniformity and leakage. Therefore, it may be of general interest to discuss in detail the impact of the structural features of the

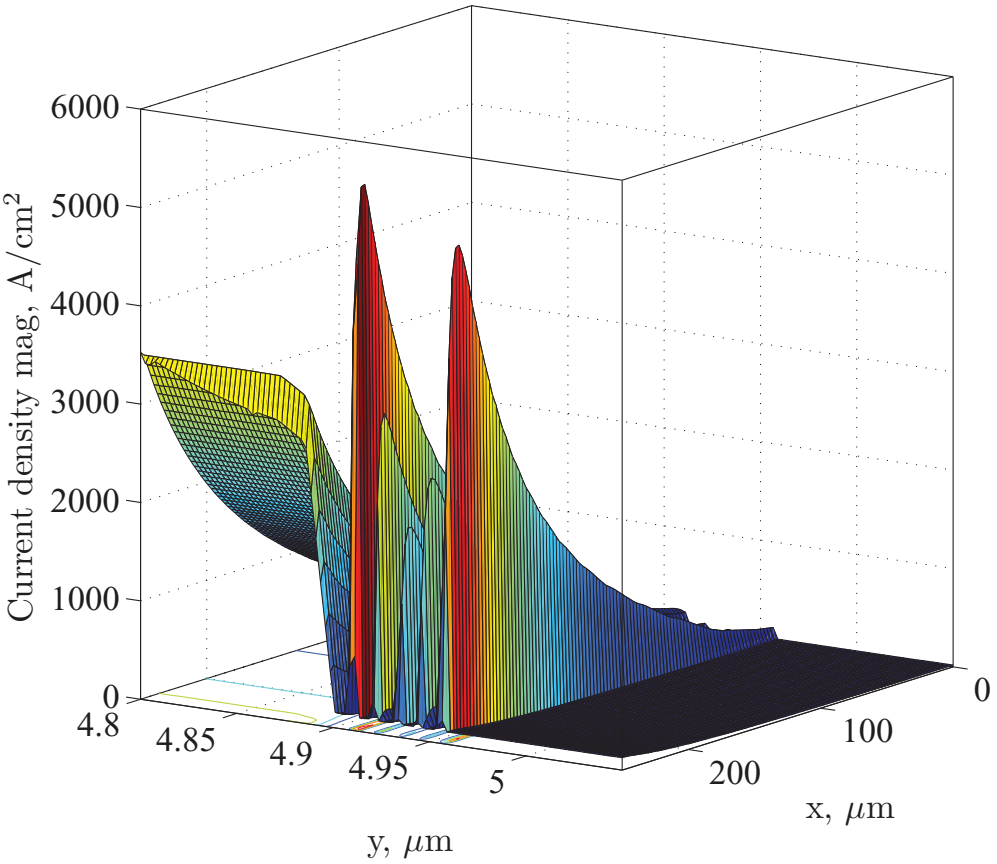

FIG. 8. Simulated modulus of the total current density in a LDD LED at $T = 15\,^{\circ}$C and $I = 100$ mA ($J = 40$ A/cm^2) as a function of the lateral coordinate x (measured from the center of the 0.5 mm-wide mesa) and of the vertical coordinate y (from the bottom of the mesa to the p side contact).

devices under examination on the calibration of the comparison between measured and simulated characteristics.[34]

First, our LEDs, as well as most non-vertical structures, are affected by nonnegligible current crowding (see e.g. Refs. 35–41). The simulated lateral profile of the vertical component of the electron current density $J_{n,\,y}(x)$ in the present devices at a current $I = 100$ mA ($J = 40$ A/cm^2) is reported in Fig. 7, where a slightly stronger crowding may be observed for increasing temperature both in the LDD and HDD case. A map of the modulus of the total current density in the mesa at the same bias level is presented in Fig. 8, where the aspect ratio of the mesa $W/H > 10^3$ is mirrored by the extensions of the considered x and y intervals. Not only the current in the vicinity of the mesa walls is significantly higher than the laterally averaged current reported in the $L(J)$ and efficiency plots, but also carrier density levels in photogenerating regions may be significantly higher near the sidewalls than in the case of uniform lateral distribution at the same current levels, as shown in Fig. 9. Hence, Auger-like effects could be strongly enhanced[37,42–44] and the corresponding C coefficient could be overestimated from an analysis of experimental L/I data neglecting crowding effects.

Second, the active region of the devices under study is not bounded by an EBL, which is usually included in order to minimize electron leakage from the active region at high current levels. However, in the present structure, the onset of efficiency droop may be observed at current densities where leakage is probably still negligible. Fig. 10 shows that, with the selected values of material parameters, numerical simulations predict essentially no electron leakage from the active region into the p-cap at a current $I = 100$ mA where droop is already significant in low-TDD structures, over

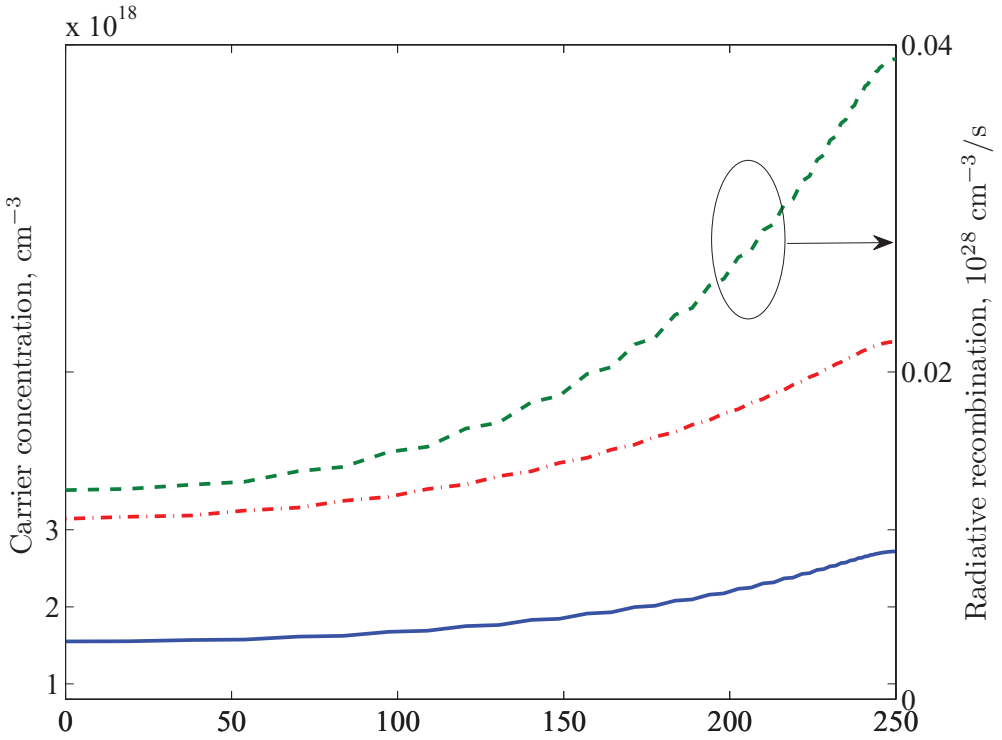

FIG. 9. Simulated electron (blue solid line) and hole (red dashed-dotted line) density and corresponding radiative recombination profile (green dashed line) as a function of the lateral coordinate x (measured from the center of the 0.5 mm-wide mesa), across the topmost QW of the active region of a LDD LED, at $T = 15\,^{\circ}\mathrm{C}$ and $I = 100$ mA ($J = 40$ A/cm^2).

the entire temperature range 15–120 °C. (As discussed in Ref. 45, electron leakage may become *less* relevant for increasing temperature.) From the same figure, the importance of current crowding may be appreciated by comparing the $J_{n,y}(y)$ profiles at different lateral coordinates.

Third, in addition to suppressing leakage, an EBL could help achieving a more uniform distribution of carriers and EL intensity among QWs, and hence a higher efficiency. An uneven vertical carrier distribution among QWs may have an effect similar to current crowding in enhancing Auger-like recombination mechanisms. In fact, lateral and vertical carrier nonuniformities translate collectively in a "reduced effective volume" of the active region, as discussed e.g. in Ref. 46. In order to check the possible effects of an EBL in the LEDs considered in the present study, a set of simulations has been performed on a structure including a 50 nm-thick $Al_{0.2}Ga_{0.8}N$ layer with a 10^{18} cm^{-3} p doping density. (See e.g. Refs. 24 and 47 for discussions on the optimal choice of EBL thickness, composition and doping level.) Little impact from the EBL insertion has been observed in the simulations, up to a current $I = 100$ mA (see Fig. 11), either on leakage current and vertical carrier distribution or on current crowding.

As a final note in this discussion of carrier density distributions, we recall that realistic device modeling requires the inclusion of temperature-dependent incomplete dopant ionization. In the present study, activation energies $E_D = 20$ meV and $E_A = 200$ meV have been assumed in GaN for Si and Mg, respectively. These energies correspond to ionized donor and acceptor densities in the n-buffer and p-cap $N_D^+ \approx 1.7 \cdot 10^{18}$, $2 \cdot 10^{18}$ cm^{-3} and $N_A^- \approx 2.7 \cdot 10^{17}$, 10^{18} cm^{-3} at $T = 15\,^{\circ}\mathrm{C}$ and $T = 120\,^{\circ}\mathrm{C}$, respectively. An example of the importance of incomplete ionization is presented in Fig. 12, where the significant increase of the fraction of ionized acceptors at $T = 120\,^{\circ}\mathrm{C}$ contributes to more uniform distributions of carriers and radiative emission among the QWs of a LDD LED,[48] which partly compensate the adverse effects of temperature on IQE through increased nonradiative recombination coefficients and decreased radiative processes.

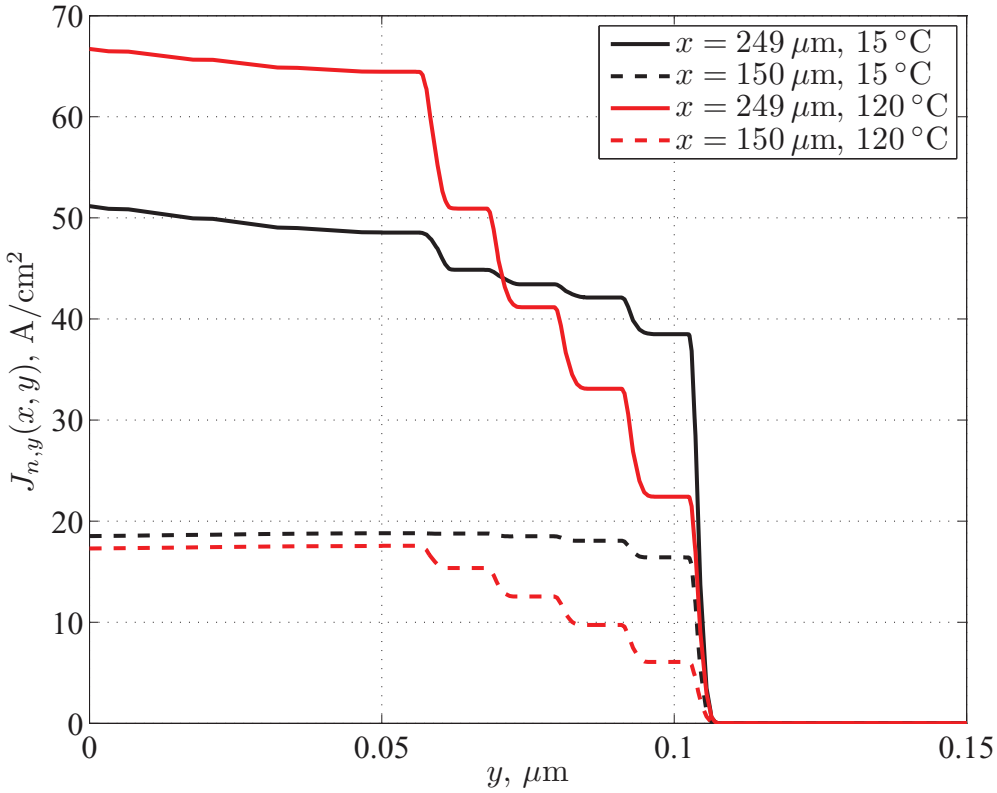

FIG. 10. Simulated vertical component of the electron current density across the active region of a LDD LED at $T = 15\,^{\circ}$C (black lines) and $T = 120\,^{\circ}$C (red lines), at an injection current $I = 100$ mA ($J = 40$ A/cm^2). The current profiles at two values of the lateral coordinate x (measured from the center of the 0.5 mm-wide mesa) are reported.

B. Structural symmetries and the 2D approximation

A seemingly trivial simulation detail is the appropriate assignement of the boundary conditions on the mesa walls. In the present 2D simulations, in order to halve the computational box, the device symmetry along the lateral direction (x) has been exploited by applying Neumann boundary conditions along a vertical axis at the center of the mesa, where the reference $x = 0$ has been taken (see Figs. 1 and 2). While the effect of this halving on the current flow across the device is obvious, the impact on the corresponding emitted optical power must be checked in order to avoid possible double counting, depending on the definition used by the CAD software for the power generated/emitted from spontaneous emission.[49]

A less trivial symmetry issue is related to the square-ring shape of the cathode contact. Since the n-side metallization surrounds the entire mesa periphery, in the presence of current crowding a fully 3D simulation should be required.[7,38,50–55] Thanks to the device symmetries and lateral dimensions, in the following Sections a quasi-3D approximation has been adopted by determining temperature-dependent correction factors $f_{J,\mathrm{ring}}(T;V) = J_{3D}(T;V)/J_{2D}(T;V)$ and $f_{L,\mathrm{ring}}(T;V) = L_{3D}(T;V)/L_{2D}(T;V)$, used to weight the 2D-simulated current density and emitted optical power when compared with the corresponding experimental values. This approximation has been validated against fully-3D simulations performed with TCAD SENTAURUS on increasingly realistic test structures (see Figs. 2 and 13). The severe current crowding predicted by both APSYS and TCAD SENTAURUS for the LED structures under consideration lead to $f_{J,\mathrm{ring}}(T;V) \approx f_{L,\mathrm{ring}}(T;V) \approx 2$ (see Fig. 14). The use of uncorrected 2D models to fit experimental results in LEDs affected by current crowding may result in significant underestimation of the Auger-like recombination coefficients, as examined in the next Section. It is worth emphasizing that, however important, this modeling error can be easily prevented, and should not be confused

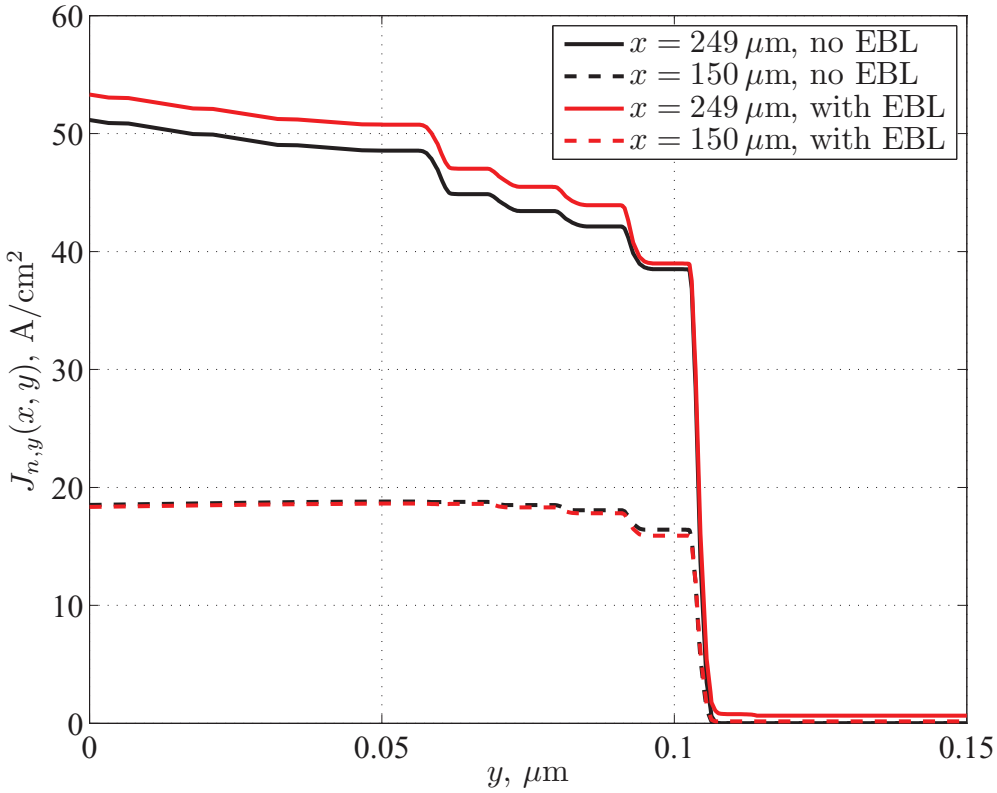

FIG. 11. Simulated vertical component of the electron current density across the active region of a LDD LED at $T = 15\,^{\circ}$C without (solid lines) and with (dashed lines) a 50 nm-thick p-doped $Al_{0.2}Ga_{0.8}N$ EBL, at an injection current $I = 100$ mA ($J = 40$ A/cm^2). The current profiles at two values of the lateral coordinate x (measured from the center of the 0.5 mm-wide mesa) are reported.

with the possible sources of *C over*estimation mentioned in Section III A (mainly concerning 1D approximations) and the most critical ones discussed in Sections V B and V C.

IV. 3D SIMULATION STUDY

Either with a charge-control model based on Eq. (1) or with a 3D numerical device simulator, it is straightforward to match a single experimental *L*/*I* curve of any given LED by adjusting the recombination parameters *ABC*. Unfortunately, such an exercise is of modest practical relevance, because of non insignificant concerns about the uniqueness of the "optimal" coefficients determined by the fitting process.

In the present study, the availability of experimental information not only on a wide range of injection currents and temperatures, but also on samples differing nominally only for their TDD (and hence for their SRH lifetimes) has allowed the definition of a large set of constraints, hopefully removing much of the arbitrariness from the optimization procedure leading to the appraisal of the recombination coefficients. As additional self-imposed restrictions, the coefficients C_n, C_p, used in the simulations to describe the Auger-like recombination rate as $R_{\mathrm{Auger}} = n^2 p C_n + n p^2 C_p$, were assumed to exhibit the approximately linear dependence on T observed in Refs. 67 and 68, while the A coefficient was assumed to be roughly proportional to N_{disl}[69] (see also the recent studies on the impact of TDD on LED efficiency presented in Refs. 63, 70–76). Auger coefficients were not forced to be the same in LDD and HDD LEDs because, although nominally identical, secondary ion mass spectrometry (SIMS) measures suggest that the QWs of the LDD devices have probably a smoother profile, which could imply a lower Auger rate.[77] The radiative recombination coefficient B was not used in the present calculations because the radiative recombination rate R_{rad} is self-consistently

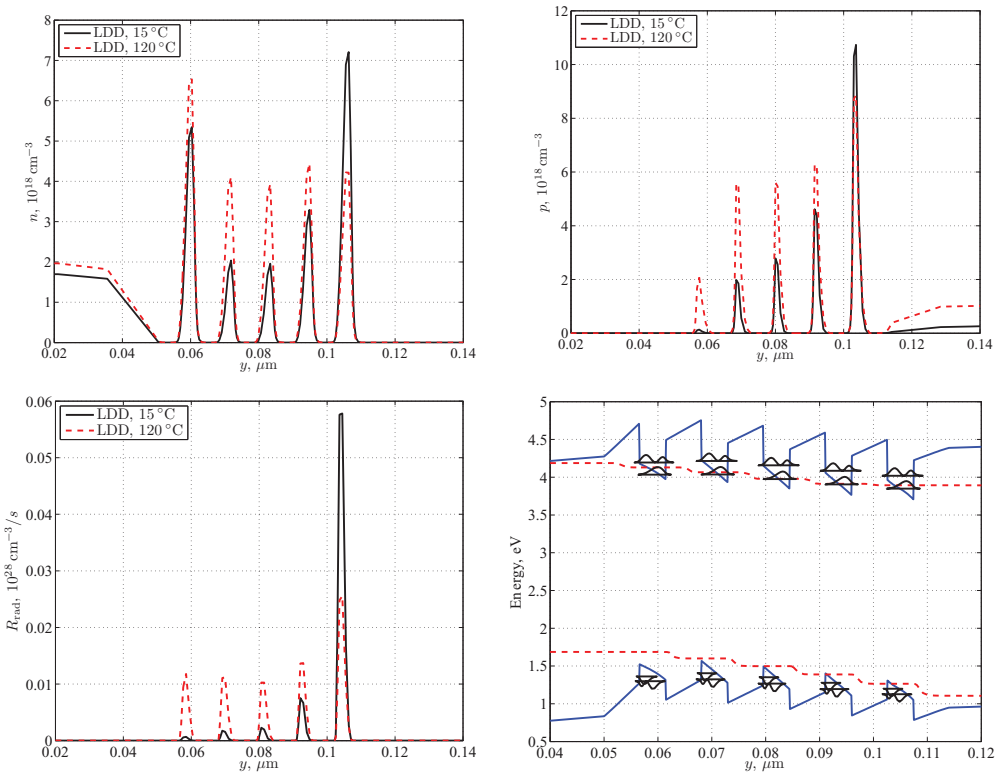

FIG. 12. Simulated electron and hole density and corresponding radiative recombination profile across the active region in $x = 240\,\mu$m at $T = 15\,^{\circ}$C (black solid lines) and $T = 120\,^{\circ}$C (red dashed lines) for a current density $J = 40$ A/cm^2 (corresponding to $I = 100$ mA) in a LDD LED. (Similar profiles have been observed in the simulation of a HDD LED.) A detail of the band diagram at $T = 15\,^{\circ}$C, $J = 40$ A/cm^2 is also presented, including the two lowest-lying subbands in each QW, the modulus of the corresponding wavefunctions, and the electron and hole quasi-Fermi levels (red dashed lines).

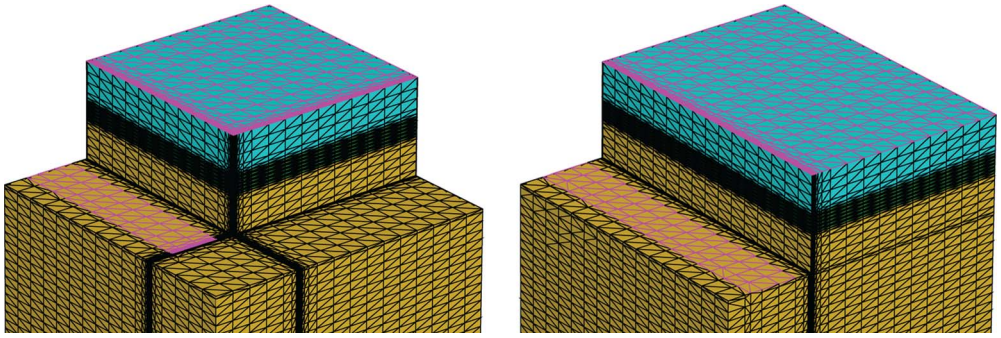

FIG. 13. Alternative 3D structures simulated in order to validate the standard 2D analysis and to estimate the correction factors $f_{J,\mathrm{ring}}$ and $f_{L,\mathrm{ring}}$. (Left) the cathode contact is placed only along the mesa walls parallel to the y axis. (Right) the entire structure is assumed to be uniform along y, in complete analogy with 2D simulations.

determined by the simulator in the active region. The optimization space was effectively limited also by the absence of an EBL and by the seeming negligible contribution of leakage in the devices under study, discussed in Section III, which remove possible effects from e.g. uncertainties in the valence band offset at the barrier/EBL interface.[45] Some effects of model and structural parameter variability will be addressed in Section V.

The "optimal" SRH lifetimes and Auger-like coefficients, determined with the nominal values of all other material parameters listed in Appendix A 1, are reported in Table I along with previous estimates of the recombination coefficients for InGaN/GaN LEDs (see also Refs. 78 and 79). Both

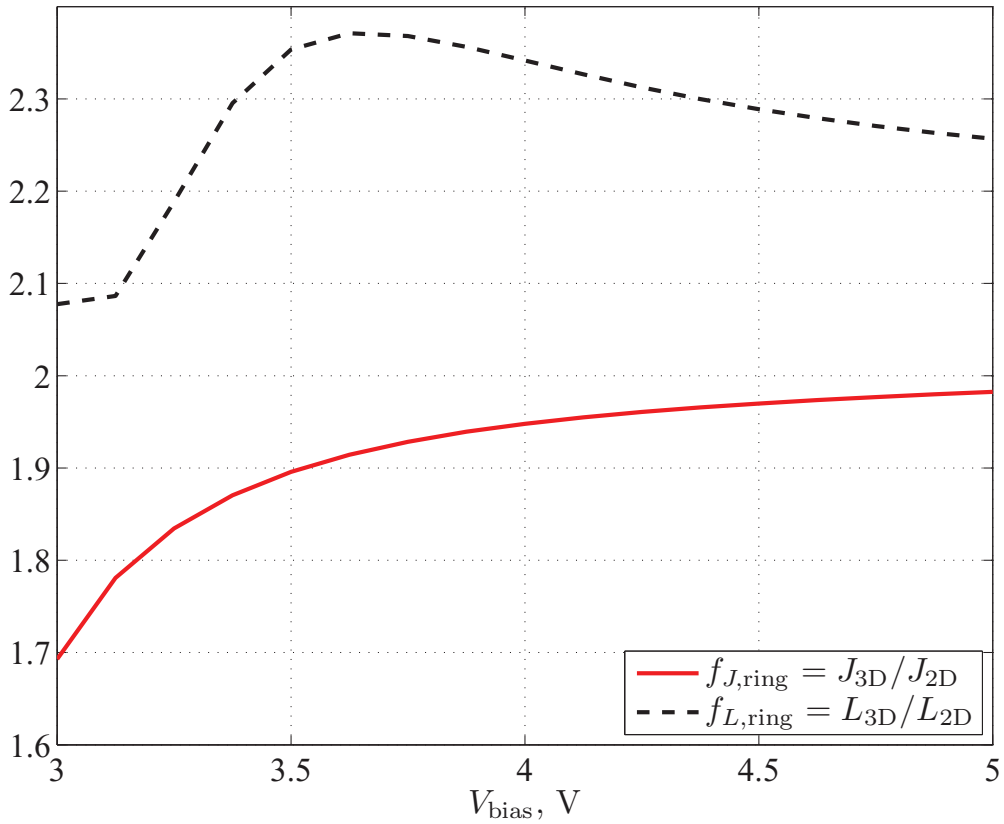

FIG. 14. Correction factors $f_{J,\text{ring}}$ and $f_{L,\text{ring}}$ at $T = 15\,^{\circ}\text{C}$ as functions of the applied bias.

TABLE I. Threading dislocation density, Shockley-Read-Hall lifetime τ_{SRH} and recombination coefficients estimated in the present study and reported in the literature for InGaN/GaN LEDs.

	N_{disl}, cm^{-2}	τ_{SRH}, ns	B, cm^3/s	C, cm^6/s	λ_{peak}, nm
LDD, 15 °C	$3 \cdot 10^8$	900		$2.7 \cdot 10^{-30}$	470
LDD, 120 °C	$3 \cdot 10^8$	90		$3.5 \cdot 10^{-30}$	470
HDD, 15 °C	$8 \cdot 10^9$	15		$5.7 \cdot 10^{-30}$	470
HDD, 120 °C	$8 \cdot 10^9$	2.7		$7.8 \cdot 10^{-30}$	470
Ref. 56	10^8	$\tau_n = 9$, $\tau_p = 46$	$2.4 \cdot 10^{-11}$	–	
Ref. 57	$5.3 \cdot 10^8$, $5.7 \cdot 10^9$	12.3 – 6.4	10^{-10}	–	440
Ref. 58	–	44	10^{-11}	10^{-30}	450
Ref. 59	$2 \cdot 10^{14}$ cm^{-3}	100	$2 \cdot 10^{-11}$	$1.5 \cdot 10^{-30}$	407
Ref. 30	–	–	10^{-10}	$8 \cdot 10^{-29}$	460
Ref. 60	–	210	$1.2 \cdot 10^{-12}$	$3.5 \cdot 10^{-31}$	green
Ref. 60	–	400	$2 \cdot 10^{-12}$	$3.5 \cdot 10^{-31}$	green
Ref. 28	–	50	$7 \cdot 10^{-11}$	10^{-29}	430
Ref. 61	–	35 – 191	–	–	460
Ref. 62	–	20 – 40	–	$5 \cdot 10^{-33}$	520
Ref. 63	$5.3 \cdot 10^8$, $5.7 \cdot 10^9$	10	–	–	
Ref. 64	–	24	$3 \cdot 10^{-12}$	$4.5 \cdot 10^{-31}$	violet
Ref. 65	–	0.2 – 1	–	$1.8 - 0.2 \cdot 10^{-31}$	
Ref. 66	–	14 – 170	$3 - 6 \cdot 10^{-12}$	$0.8 - 1 \cdot 10^{-31}$	440 – 470

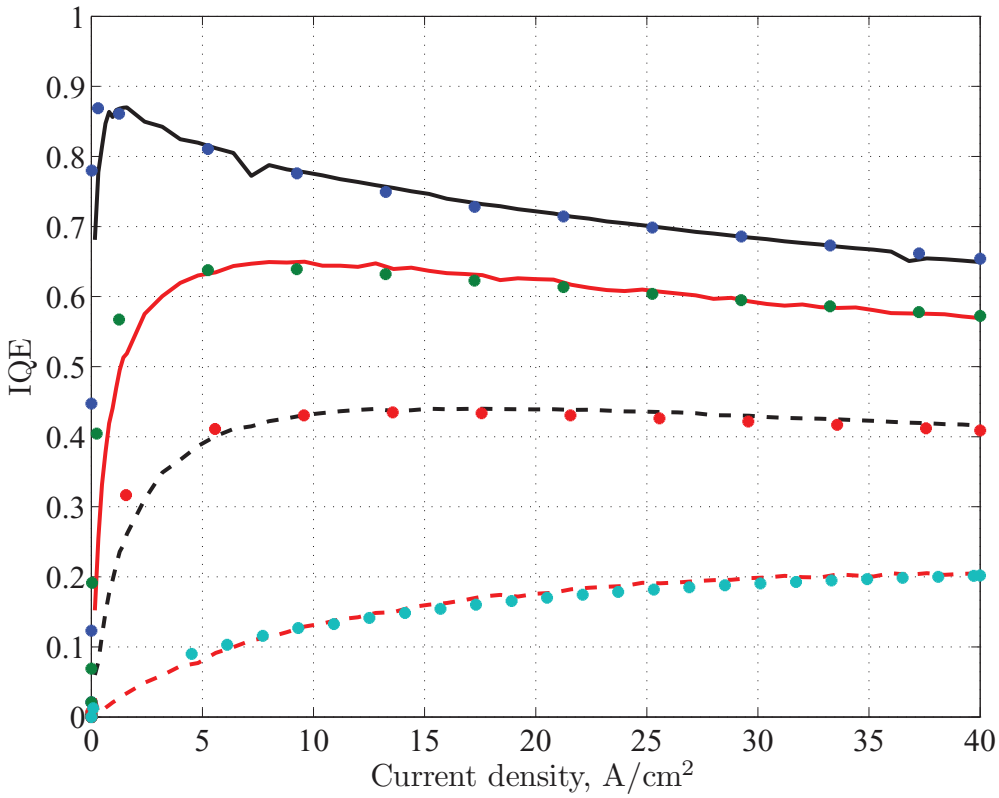

FIG. 15. Normalized simulated IQE (symbols) and measured *L*/*I* (lines) as functions of the injection current density in a LDD (solid lines) and HDD (dashed lines) LED at $T = 15\,^{\circ}$C (black lines) and $T = 120\,^{\circ}$C (red lines). The non-normalized value of the maximum simulated IQE is 91%.

in the LDD and HDD case, the ratio between the present estimates of the C coefficients at 15 °C and 120 °C is approximately equal to the ratio between the corresponding absolute temperatures. If current crowding effects were neglected when comparing experiments and simulations, i.e. if $f_{J,\mathrm{ring}} \approx f_{L,\mathrm{ring}} \approx 1$ were assumed, C would be underestimated by a factor ≈1.5÷1.9 (see comment at the end of Section III A).

A comparison between measured and simulated IQE(J; T) with the "optimal" τ_{SRH} and C values is shown in Fig. 15. Fig. 16 reports the experimental and simulated EL spectra for different temperatures and currents in a LDD and HDD LED, respectively; for recent comparable experimental studies on the dependence of λ_{peak} on current and temperature, see e.g. Refs. 80–82. It is worth mentioning that, for a realistic description of radiative emission, it has been essential here to take into account the broadening of interband transitions due to inhomogeneities in QW thickness and composition.[83–85] This can be appreciated from Fig. 17, which compares simulated EL spectra at different temperatures with and without broadening in a LDD LED. The spectra are normalized, as the adopted model for broadening does not affect the total generated optical power or the IQE. The inclusion of many-body Coulomb interactions[86–92] as implemented in the present versions of the simulators has not resulted, with the exception of E_g renormalization, in a real improvement in their predictive capabilities, due to the large set of widely-adjustable empirical parameters involved in the corresponding models.

V. UNCERTAINTY ASSESSMENT

While a systematic uncertainty quantification is beyond the reach of the present analysis of GaN-based LEDs, we will attempt here a critical discussion of the results derived in Section IV. Our focus will be on what we consider the weakest points of the DD modeling framework, whose combined

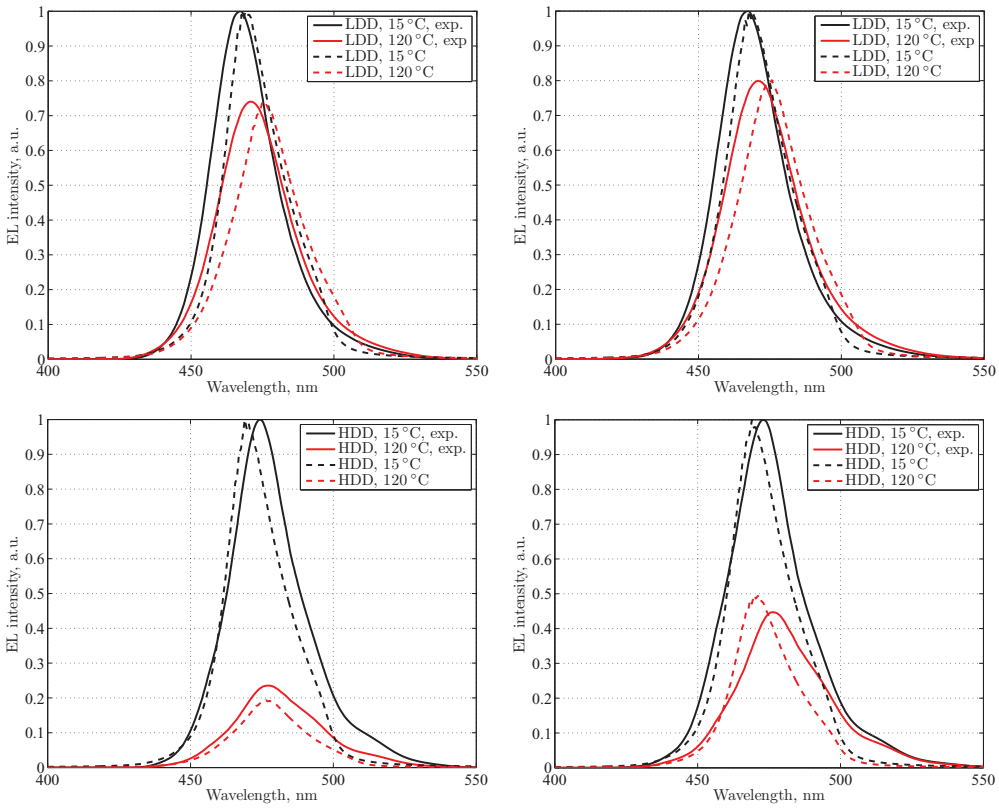

FIG. 16. Experimental (solid lines) and simulated (dashed lines) EL spectra in a LDD (top) and HDD (bottom) LED at $T = 15\,^{\circ}\mathrm{C}$ (black lines) and $T = 120\,^{\circ}\mathrm{C}$ (red lines) for a current density (left) $J = 8$ A/cm^2 and (right) $J = 40$ A/cm^2 (corresponding to $I = 20$ mA and $I = 100$ mA, respectively).

limitations could determine, in particular, a severe overestimation of the Auger-like coefficient also beyond the present case study.

A. Carrier transport across the active region

In the previous analysis, a standard DD model for carrier transport across the active region has been adopted, not including carrier flyover (ballistic transport)[13–15,24] or Auger-induced leakage.[17] The dependence of carrier velocity on the electric field has been approximated with a Canali-like description[93] using state-of-the-art model parameters.[94–96] We have also experimented modified transferred-electron models[97] as well as hydrodynamic and energy-balance descriptions,[98] without noticeable improvements in the predictive capabilities of the simulator.

Among "quantum–corrected" transport models, a well-established approach available in most commercial simulators involves the use of separate continuity equations for carriers in unconfined bulk states (3D) and in bound QW states (2D).[99] This split-state description, separating the 3D and 2D quasi-Fermi levels in the active region, requires the definition of an appropriate recombination-like coupling term, in turn involving a set of time constants τ_{QW} associated with the capture/escape processes.[100,101] A recent body of work using split-state models in InGaN-based LEDs[16,24,102,103] suggests that capture time constants $\tau_{QW} \approx 10^{-6}$ s are required in order to obtain realistic IQE values if other loss mechanisms (Auger recombination in particular) are assumed to be negligible. The need of such long τ_{QW} has led the authors of Ref. 24 to rule out incomplete QW capture (at least, in its present formulation) as a possible droop mechanism. A similar conclusion seems appropriate also in the case of the present LED structures, since not only low capture rates have to

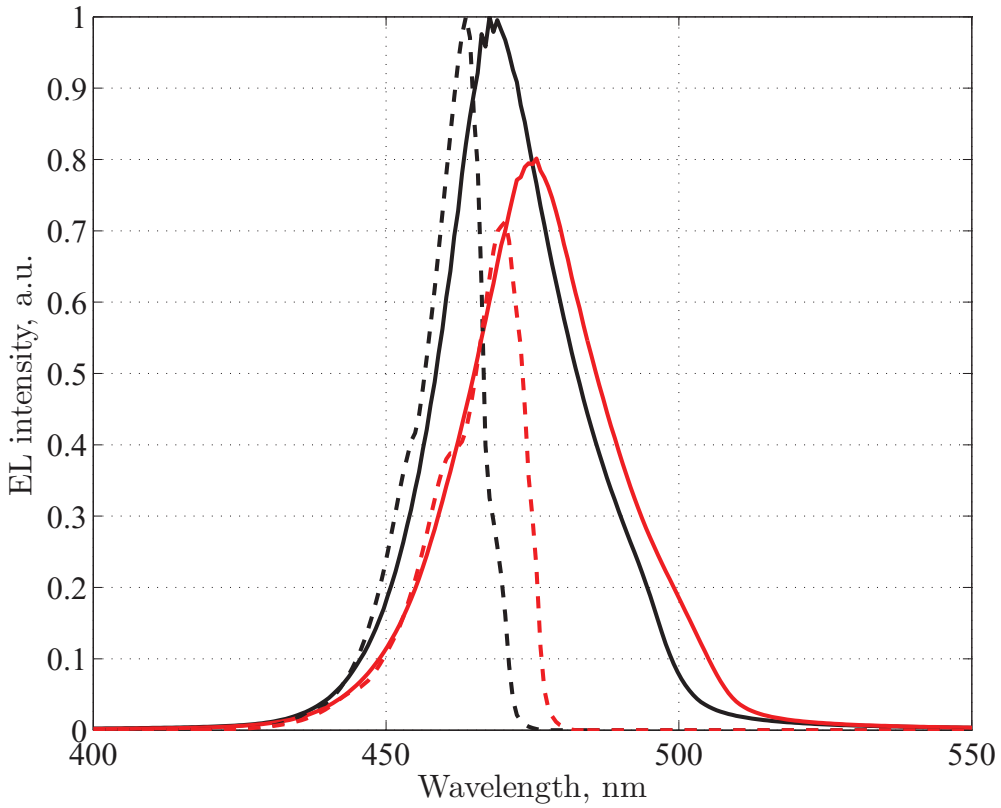

FIG. 17. Simulated EL spectra in a LDD LED at $T = 15\,^{\circ}$C (black lines) and $T = 120\,^{\circ}$C (red lines) for a current density $J =$ 40 A/cm^2 (corresponding to $I = 100$ mA) with (solid lines) and without (dashed lines) including inhomogeneous broadening.

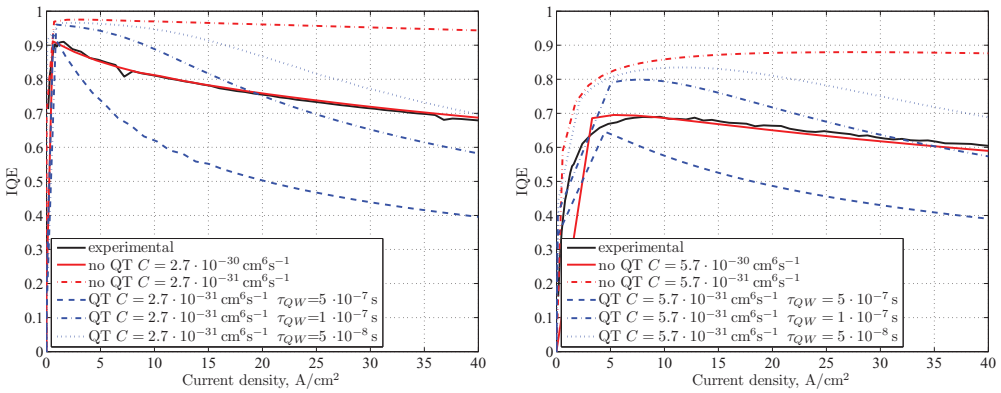

FIG. 18. Simulated (non-normalized) IQE at $T = 15\,^{\circ}$C (left) and $T = 120\,^{\circ}$C (right) as a function of the injection current density in a LDD LED for different values of the capture time τ_{QW} and a C coefficient set to a value equal to 1/10 of the corresponding "best fit" value listed in Table I. Also reported, as a reference, are the experimental *L*/*I* (black solid lines) and the corresponding "optimal" simulated IQE with no split-state model (red solid lines) rescaled from Fig. 15.

be assumed ($\tau_{QW} \approx 10^{-7}$ s), but also the IQE dependence on current density and temperature cannot be satisfactorily reproduced when long τ_{QW} are used in the simulations (see Fig. 18).

B. Spontaneous emission

In the previous Sections, spontaneous emission has been calculated with the present APSYS default parameters of the valence band $\boldsymbol{k} \cdot \boldsymbol{p}$ Hamiltonian, reported in Table II and derived from

TABLE II. Material parameters of GaN and InN used in the present simulations.

Parameter	GaN	InN
a, Å	3.1892	3.5446
c, Å	5.185	5.718
E_g at $T = 0$ K, eV	3.507	0.735
α, meV K^{-1}	0.909	0.245
β, K	830	624
χ, eV	4.07	5.9272
Δ_{so}, meV	14	1
Δ_{cr}, meV	19	41
ε_0	9.5	15
$m_e^{\parallel}$	0.20	0.065
$m_e^{\perp}$	0.20	0.065
A_1	−6.56	−8.21
A_2	−0.91	−0.68
A_3	5.65	7.57
A_4	−2.83	−5.23
A_5	−3.13	−5.11
A_6	−4.86	−5.96
D_1, eV	−3.0	−3.0
D_2, eV	3.6	3.6
D_3, eV	8.82	8.82
D_4, eV	−4.41	−4.41
D_5, eV	−4.0	−2.33
D_6, eV	−5.0770	−0.3536
c_{11}, GPa	390	271
c_{12}, GPa	145	124
c_{13}, GPa	106	92
c_{33}, GPa	398	224
c_{44}, GPa	105	46
P_{SP}, C m^{-2}	−0.034	−0.042
μ_n, cm^2 V^{-1}s^{-1}	300	
μ_p, cm^2 V^{-1}s^{-1}	10	

Ref. 105 for GaN and Ref. 106 for InN. However widely adopted, those parameter values are affected by a considerable uncertainty, which directly affects the LED characteristics. As a demonstration of the importance for device simulation of the description of the valence bands near Γ, Fig. 19 compares the computed IQE and EL spectra corresponding to the default band parameters and to a more recent $\boldsymbol{k}\cdot\boldsymbol{p}$ model derived from many-body perturbation theory in the G_0W_0 approximation.[104] The newer $\boldsymbol{k}\cdot\boldsymbol{p}$ model, in particular its larger crystal-field splitting of GaN, leads to a nonnegligible decrease in both the EL intensity and the IQE at all injection currents; if used in Section IV, it would have led to significantly lower "optimal" estimates of both the A and C coefficients.

C. Auger recombination and Auger-related processes

Fig. 20, reporting the simulated IQE as a function of the injection current for different values of the C Auger-like coefficient and of the TDD-SRH-like lifetime, could be used to assert our confidence in the nonradiative recombination coefficients estimated from the analysis presented in Section IV.

The order of magnitude of our A and C values is indeed in general agreement with several simulation studies discussing Auger effects on LED droop[3,4,23,24,47,107] and recent experimental studies on Auger recombination, focusing on its temperature[108] and composition[65,66] dependence and reaffirming the importance of Auger processes in the blue spectral range. Notably, the Auger-like coefficient determined in the present LED study is increasing with temperature, i.e. it would

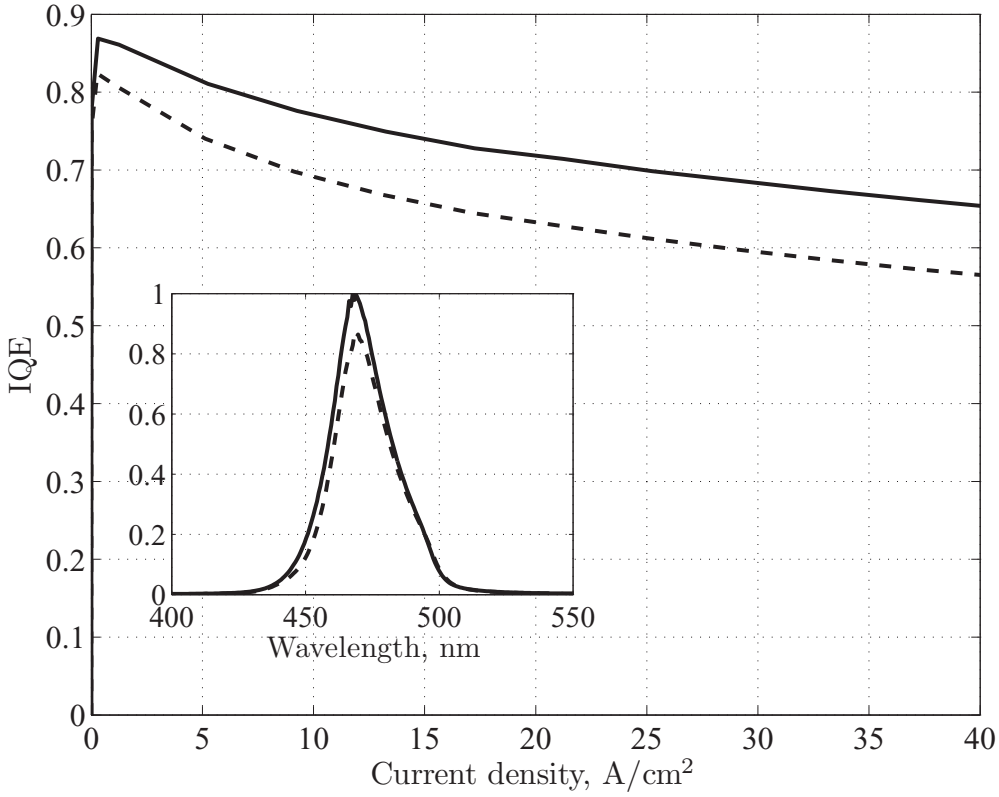

FIG. 19. Simulated (non-normalized) IQE at $T = 15\,^{\circ}$C as a function of the injection current density in a LDD LED for the default band parameters reported in Table II (solid line) and the alternative values proposed in Ref. 104 (dashed line). The corresponding EL spectra at $J = 40$ A/cm^2 ($I = 100$ mA) are reported in the inset.

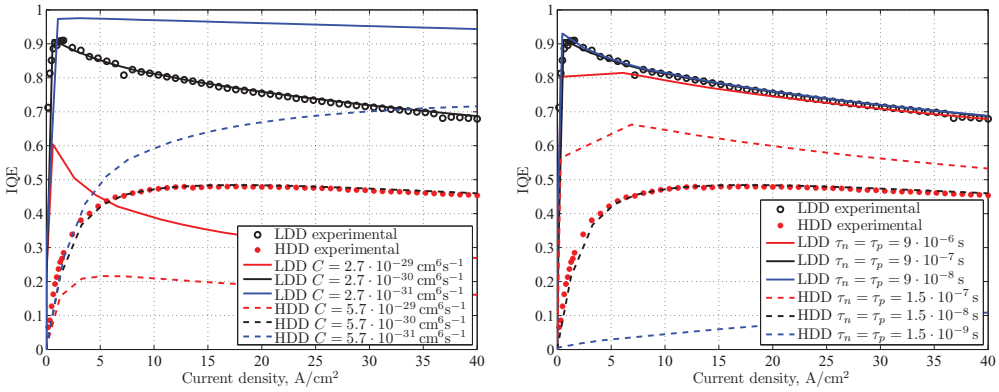

FIG. 20. Simulated (non-normalized) IQE at $T = 15\,^{\circ}$C as a function of the injection current density for different values of the C Auger-like coefficient (left) and of the TDD-related SRH lifetimes (right). Experimental (normalized) L/I values are reported as references.

be compatible with Auger processes in InGaN/GaN QWs rather than with density-activated defect recombination or leakage from the active region, both decreasing with increasing temperature.[26,29,45]

However, in our opinion, an accurate determination of the actual Auger rates remains elusive to a combined experimental and simulation analysis based on state-of-the-art DD-based optoelectronic CAD tools, not only because the applicability of the *ABC* model to QWs is somehow questionable,[27] but also on account of possible enhancements of Auger recombination by Coulomb interactions[109] and of the significant uncertainties on the radiative losses (see Section V B and Ref. 92), which are

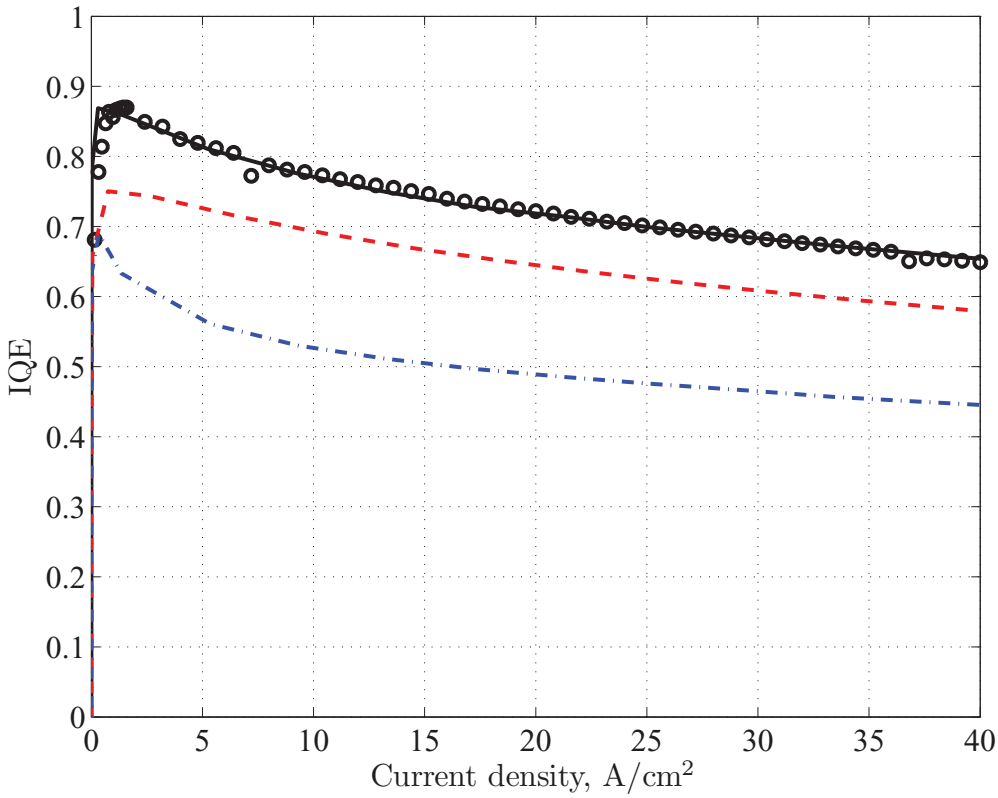

FIG. 21. Simulated (non-normalized) IQE at $T = 15\,^{\circ}$C as a function of the injection current density for different thickness and In molar fraction of the QWs: 5 nm, 15% (solid); 2 nm, 15% (dashed), 2 nm, 20% (dashed-dotted). Experimental (normalized) *L*/*I* values are reported as references.

also strongly affected by the microscopic details of the MQW heterostructures. If the relationship between recombination coefficients in bulk and in QWs is not better explored, beyond the attempt presented in Ref. 110, the very "portability" of C between different devices is dubious.[22] Direct calculations of Auger recombination in QW structures, usually based on $\boldsymbol{k}\cdot\boldsymbol{p}$ models, agree in suggesting the importance of QW composition profiles[77,111] and polarization fields[112] on the direct process rates. Moreover, fluctuations of the In molar fraction across the active region[113,114] could have significant effects on both leakage and Auger recombination.[115,116]

Even assuming an ideally uniform QW profile across the device, as we have done in the previous Sections, the determination of C is significantly influenced by the uncertainties on QW thickness and composition. As an example, Fig. 21 compares the IQE corresponding to the nonradiative recombination coefficients estimated in the previous Section (with the "worst case" 5 nm-thick $In_{0.15}Ga_{0.85}N$ QWs) and the results obtained assuming thinner (2 nm) and deeper (up to 0.20 In molar fraction) QWs. Electron leakage and current crowding are minimally affected by these changes, while the use of the worst-case-geometry A and C coefficients with the thinner QWs leads to a significantly larger droop, and the C estimate could be reduced approximately by a factor 3 with 2 nm-thick $In_{0.2}Ga_{0.8}N$ QWs.

In addition to these uncertainties, recent modeling work[17] suggests that experimentally-derived C values could overestimate the real ones up to a factor 2 since they do not take into account Auger-induced leakage effects. Finally, possible non-Auger contributions to the Auger-like coefficients could derive from photon quenching mechanisms[117] or from strong nolinearities in the n-dependence of SRH-like recombination processes determined by multiple-level defects,[76] and would further hamper the discrimination between Auger and other nonradiative mechanisms from an analysis of the LED characteristics.

VI. CONCLUSIONS

After a discussion of some important pitfalls stemming from 1D and 2D simulation of LED structures – foremost the possible incorrect determination of the C coefficient in the presence of current crowding – we have presented a combined experimental and simulative study on InGaN/GaN LEDs where a seeming excellent match between measured and calculated IQE characteristics and EL spectra has been achieved over a wide range of temperatures and operating currents, by using as the only fitting parameters the A and C coefficients conventionally associated with SRH-like and Auger recombination.

However, even if the present study is based on a large and consistent set of experimental data, we have shown that the estimates of A and especially C are affected by large error margins because of the many sources of uncertainty, related not only to device structure and technological details (distribution, activation and ionization of dopant species; composition profiles of QWs and barriers in the active region; uniformity of contacts; parasitic resistances and other interface effects; etc.) and to material parameters (band offsets and polarization charges at heterojunctions, energy gap and electronic structure of GaN and InGaN in presence of strain, defects, nonideal interfaces, etc.), but also to a possibly inadequate description of microscopic processes in the active region (radiative recombination, intra- and inter-subband carrier scattering, capture/escape between bound and unbound states, carrier flyover and tunneling etc.) and of their problematic inclusion in a device-level DD CAD suite.

These uncertainties are compounded by the nontrivial relationship between the bulk C coefficient used in the simulations and the corresponding 2D Auger rate, and by the possible role played by non-Auger recombination mechanisms with a strong nonlinear dependence on the carrier density; a calculation approach for QW structures "beyond $\boldsymbol{k}\cdot\boldsymbol{p}$" is needed[68,118,119] also in order to take advantage of possible polarization-engineering opportunities.[112,120,121]

The prime requisite for a better understanding of experimental information is probably an improved description of carrier transport across the active region. Promising efforts are represented by momentum-resolved models[23,122] and analytic-band Monte Carlo (MC) transport simulations,[123] but the need for a full-band MC approach (FBMC, possibly integrated with microscopic models of radiative and nonradiative recombination processes) is apparent, especially after the recent debate following the proposed identification of Auger recombination as the dominant mechanism in droop from electron emission spectroscopy experiments,[124] where FBMC analysis has suggested that the LED structure under investigation was probably unsuitable to recover an Auger signature.[125]

ACKNOWLEDGMENTS

The authors thank Simone Chiaria, Andrew Phillips and Michel Lestrade for useful discussions, Simone Vaccari and Marco Ferretti for their contribution to the experimental characterization. The work at Politecnico di Torino and Boston University was supported in part by the U.S. Army Research Laboratory through the Collaborative Research Alliance (CRA) for MultiScale multidisciplinary Modeling of Electronic materials (MSME).

APPENDIX

1. Model parameters

The nominal values of the material parameters used in the present simulations are listed in Table II (see also Refs. 47, 106, 126, and 127), where a and c are the lattice constants, E_g is the energy gap, α and β are the coefficients of the Varshni model for the temperature dependence of E_g,[106] χ is the electron affinity, Δ_{so} and Δ_{cr} are the spin-orbit and crystal-field splitting, ε_0 is the relative dielectric constant, $m_e^{\parallel}$ and $m_e^{\perp}$ are the longitudinal and transverse components of the electron effective mass, $A_1 \ldots A_6$ are the Luttinger parameters of the $\boldsymbol{k}\cdot\boldsymbol{p}$ Hamiltonian, $D_1 \ldots D_6$ are the valence band deformation potentials, $c_{11} \ldots c_{44}$ are the elastic constants for wurtzite materials, P_{SP} is the spontaneous polarization, $\mu_{n,p}$ are the electron and hole mobilities (assumed to be independent of temperature, ionized impurity densities, and In molar fraction). A linear interpolation between

the values of the binary compounds has been used for all $In_xGa_{1-x}N$ parameters, with the exception of E_g and P_{SP}, where a quadratic correction $x(1-x)b$ has been included, with bowing factors b equal to 3.0 eV and -0.038 C m^{-2}, respectively. A conduction band offset $\Delta E_c/\Delta E_g = 0.67$ has been assumed for all heterojunctions, regardless of the In molar fraction.

[1] M. H. Crawford, IEEE J. Select. Topics Quantum Electron. **15**, 1028 (2009).
[2] A. Laubsch, M. Sabathil, W. Bergbauer, M. Strassburg, H. Lugauer, M. Peter, S. Lutgen, N. Linder, K. Streubel, J. Hader, J. V. Moloney, B. Pasenow, and S. W. Koch, Phys. Stat. Sol. (c) **6**, S913 (2009).
[3] Ü. Özgür, H. Liu, X. Li, X. Ni, and H. Morkoç, Proc. IEEE **98**, 1180 (2010).
[4] J. Piprek, Phys. Stat. Sol. (a) **207**, 2217 (2010).
[5] J. Cho, E. F. Schubert, and J. K. Kim, Laser & Photon. Rev. **7**, 408 (2013).
[6] G. Verzellesi, D. Saguatti, M. Meneghini, F. Bertazzi, M. Goano, G. Meneghesso, and E. Zanoni, J. Appl. Phys. **114**, 071101 (2013).
[7] J. Piprek, and S. Li, in *Optoelectronic Devices: Advanced Simulation and Analysis*, edited by J. Piprek (Springer, New York, 2005) Chap. 10, pp. 293–312.
[8] S. Y. Karpov, in *Nitride Semiconductor Devices: Principles and Simulation*, edited by J. Piprek (Wiley-VCH Verlag, Weinheim, 2007) Chap. 14, pp. 303–325.
[9] N. I. Bochkareva, V. V. Voronenkov, R. I. Gorbunov, A. S. Zubrilov, Y. S. Lelikov, P. E. Latyshev, Y. T. Rebane, A. I. Tsyuk, and Y. G. Shreter, Appl. Phys. Lett. **96**, 133502 (2010).
[10] S. Huang, Y. Xian, B. Fan, Z. Zheng, Z. Chen, W. Jia, H. Jiang, and G. Wang, J. Appl. Phys. **110**, 064511 (2011).
[11] H. Zhao, G. Liu, R. A. Arif, and N. Tansu, Semiconductor Sci. Tech. **54**, 1119 (2010).
[12] T.-S. Kim, B.-J. Ahn, Y. Dong, K.-N. Park, J.-G. Lee, Y. Moon, H.-K. Yuh, S.-C. Choi, J.-H. Lee, S.-K. Hong, and J.-H. Song, Appl. Phys. Lett. **100**, 071910 (2012).
[13] X. Ni, X. Li, J. Lee, S. Liu, V. Avrutin, Ü. Özgür, H. Morkoç, and A. Matulionis, J. Appl. Phys. **108**, 033112 (2010).
[14] M. V. Kisin and H. S. El-Ghoroury, Phys. Stat. Sol. (c) **8**, 2264 (2011).
[15] Ü. Özgür, X. Ni, X. Li, J. Lee, S. Liu, S. Okur, V. Avrutin, A. Matulionis, and H. Morkoç, Semiconductor Sci. Tech. **26**, 014022 (2011).
[16] C. S. Xia, Z. M. S. Li, Y. Sheng, L. W. Cheng, W. D. Hu, and W. Lu, Opt. Quantum Electron. **45**, 597 (2013).
[17] M. Deppner, F. Römer, and B. Witzigmann, Phys. Stat. Sol. RRL **6**, 418 (2012).
[18] H. Li, X. Liu, J. Wang, D. Jin, H. Zhang, S. Yang, S. Liu, W. Mao, Y. Hao, Q. Zhu, and Z. Wang, J. Appl. Phys. **112**, 113712 (2012).
[19] L. Dong, J. V. Mantese, V. Avrutin, Ü. Özgür, H. Morkoç, and S. P. Alpay, J. Appl. Phys. **114**, 043715 (2013).
[20] S.-I. Park, J.-I. Lee, D.-H. Jang, H.-S. Kim, D.-S. Shin, H.-Y. Ryu, and J.-I. Shim, IEEE J. Quantum Electron. **48**, 500 (2012).
[21] M. A. Caro, S. Schulz, and E. P. O'Reilly, Phys. Rev. B **88**, 214103 (2013).
[22] P. Blood, IEEE J. Quantum Electron. **36**, 354 (2000).
[23] W. W. Chow, Opt. Express **19**, 21818 (2011).
[24] D. Saguatti, L. Bidinelli, G. Verzellesi, M. Meneghini, G. Meneghesso, E. Zanoni, R. Butendeich, and B. Hahn, IEEE Trans. Electron Devices **59**, 1402 (2012).
[25] I.-G. Choi, D.-P. Han, J. Yun, K. S. Kim, D.-S. Shin, and J.-I. Shim, Appl. Phys. Express **6**, 052105 (2013).
[26] J. Hader, J. V. Moloney, and S. W. Koch, Appl. Phys. Lett. **99**, 181127 (2011).
[27] J. Hader, J. V. Moloney, and S. W. Koch, in *SPIE Photonics West, Physics and Simulation of Optoelectronic Devices XIV*, Vol. 6115, Proceedings of the SPIE (San Jose, CA, 2006) p. 61151T.
[28] A. David and M. J. Grundmann, Appl. Phys. Lett. **96**, 103504 (2010).
[29] J. Hader, J. V. Moloney, and S. W. Koch, Appl. Phys. Lett. **96**, 221106 (2010).
[30] Q. Dai, Q. Shan, J. Wang, S. Chhajed, J. Cho, E. F. Schubert, M. H. Crawford, D. D. Koleske, M.-H. Kim, and Y. Park, Appl. Phys. Lett. **97**, 133507 (2010).
[31] G.-B. Lin, D. Meyaard, J. Cho, E. F. Schubert, H. Shim, and C. Sone, Appl. Phys. Lett. **100**, 161106 (2012).
[32] G.-B. Lin, Q. Shan, A. J. Birkel, J. Cho, E. F. Schubert, M. H. Crawford, K. R. Westlake, and D. D. Koleske, Appl. Phys. Lett. **101**, 241104 (2012).
[33] Y. Lin, Y. Zhang, Z. Liu, L. Su, J. Zhang, T. Wei, and Z. Chen, Appl. Phys. Lett. **101**, 252103 (2012).
[34] All simulation results discussed in Section III have been determined with the "optimal" SRH lifetimes and Auger coefficients listed in Table I.
[35] X. Guo and E. F. Schubert, J. Appl. Phys. **90**, 4191 (2001).
[36] H. Kim, S.-J. Park, and H. Hwang, IEEE Trans. Electron Devices **48**, 1065 (2001).
[37] V. K. Malyutenko, S. S. Bolgov, and A. D. Podoltsev, Appl. Phys. Lett. **97**, 251110 (2010).
[38] Y. Y. Kudryk and A. V. Zinovchuk, Semiconductor Sci. Tech. **26**, 095007 (2011).
[39] K.-S. Lee, Phys. Stat. Sol. (a) **209**, 2630 (2012).
[40] V. Malyutenko, S. Bolgov, and A. Tykhonov, IEEE Photon. Technol. Lett. **24**, 1124 (2012).
[41] Y. Zhang, H. Zheng, E. Guo, Y. Cheng, J. Ma, L. Wang, Z. Liu, X. Yi, G. Wang, and J. Li, J. Appl. Phys. **113**, 014502 (2013).
[42] Y. Y. Kudryk, A. K. Tkachenko, and A. V. Zinovchuk, Semiconductor Sci. Tech. **27**, 055013 (2012).
[43] C.-K. Li and Y.-R. Wu, IEEE Trans. Electron Devices **59**, 400 (2012).
[44] E. Jung, S. Kim, and H. Kim, IEEE Electron Device Lett. **34**, 277 (2013).
[45] J. Piprek and S. Li, Opt. Quantum Electron. **42**, 89 (2010).
[46] H.-Y. Ryu, D.-S. Shin, and J.-I. Shim, Appl. Phys. Lett. **100**, 131109 (2012).

[47] S. Chiaria, E. Furno, M. Goano, and E. Bellotti, IEEE Trans. Electron Devices **57**, 60 (2010).
[48] M. Meneghini, S. Vaccari, A. Garbujo, N. Trivellin, D. Zhu, C. J. Humphreys, M. Calciati, M. Goano, F. Bertazzi, G. Ghione, E. Bellotti, G. Meneghesso, and E. Zanoni, Japan. J. Appl. Phys. **52**, 08JG09 (2013).
[49] In the following, the total optical power P_{op} generated *inside* the active region has been taken into account to determine the internal quantum efficiency (IQE), but for better consistency with the experimental *L/I* curves one could consider only the power emitted from the top surface of the mesa.
[50] J. Piprek, T. M. Katona, S. P. DenBaars, and S. Li, in *SPIE Photonics West, Light-Emitting Diodes: Research, Manufacturing, and Applications VIII*, Vol. 5366, Proceedings of the SPIE (San Jose, CA, 2004) pp. 127–136.
[51] S. Li, Z. Q. Li, O. Shmatov, C. S. Xia, and W. Lu, in *2005 MRS Fall Meeting*, Vol. 892, Materials Research Society Symposium Proceedings (MRS, 2005) pp. 0892–FF12–12.
[52] Y. Sheng, O. Shmatov, and Z. M. S. Li, in *6th International Conference on Numerical Simulation of Optoelectronic Devices (NUSOD '06)* (Singapore, 2006) pp. 19–20.
[53] M. Othman, S. Ahmad, F. Sa'ad, A. Alias, A. Aziz, and M. Hashim, in *2012 IEEE International Conference on Control System, Computing and Engineering (ICCSCE)* (Penang, Malaysia, 2012) pp. 530–534.
[54] Y. Sheng, C. S. Xia, Z. M. S. Li, and L. W. Cheng, in *12th International Conference on Numerical Simulation of Optoelectronic Devices (NUSOD 2012)* (Shanghai, China, 2012) pp. 23–24.
[55] C.-K. Li, H.-C. Yang, T.-C. Hsu, Y.-J. Shen, A.-S. Liu, and Y.-R. Wu, J. Appl. Phys. **113**, 183104 (2013).
[56] K. A. Bulashevich, V. F. Mymrin, S. Y. Karpov, I. Zhmakin, and A. Zhmakin, J. Comp. Phys. **213**, 214 (2006).
[57] M. F. Schubert, S. Chhajed, J. K. Kim, E. F. Schubert, D. D. Koleske, M. H. Crawford, S. R. Lee, A. J. Fischer, G. Thaler, and M. A. Banas, Appl. Phys. Lett. **91**, 231114 (2007).
[58] M. Meneghini, N. Trivellin, G. Meneghesso, E. Zanoni, U. Zehnder, and B. Hahn, J. Appl. Phys. **106**, 114508 (2009).
[59] M. Zhang, P. Bhattacharya, J. Singh, and J. Hinckley, Appl. Phys. Lett. **95**, 201108 (2009).
[60] A. Laubsch, M. Sabathil, J. Baur, M. Peter, and B. Hahn, IEEE Trans. Electron Devices **57**, 79 (2010).
[61] D. S. Meyaard, Q. Shan, Q. Dai, J. Cho, E. F. Schubert, M.-H. Kim, and C. Sone, Appl. Phys. Lett. **99**, 041112 (2011).
[62] H. Zhao, G. Liu, J. Zhang, J. D. Poplawsky, V. Dierolf, and N. Tansu, Opt. Express **19**, A991 (2011).
[63] S. Chhajed, J. Cho, E. F. Schubert, J. K. Kim, D. D. Koleske, and M. H. Crawford, Phys. Stat. Sol. (a) **208**, 947 (2011).
[64] W. G. Scheibenzuber, U. T. Schwarz, L. Sulmoni, J. Dorsaz, J.-F. Carlin, and N. Grandjean, J. Appl. Phys. **109**, 093106 (2011).
[65] M. Brendel, A. Kruse, H. Jönen, L. Hoffmann, H. Bremers, U. Rossow, and A. Hangleiter, Appl. Phys. Lett. **99**, 031106 (2011).
[66] D. Schiavon, M. Binder, M. Peter, B. Galler, P. Drechsel, and F. Scholz, Phys. Stat. Sol. (b) **250**, 283 (2013).
[67] F. Bertazzi, M. Goano, and E. Bellotti, Appl. Phys. Lett. **101**, 011111 (2012).
[68] F. Bertazzi, X. Zhou, M. Goano, G. Ghione, and E. Bellotti, Appl. Phys. Lett. **103**, 081106 (2013).
[69] S. Y. Karpov and Y. N. Makarov, Appl. Phys. Lett. **81**, 4721 (2002).
[70] T. Langer, A. Kruse, F. A. Ketzer, A. Schwiegel, L. Hoffmann, H. Jönen, H. Bremers, U. Rossow, and A. Hangleiter, Phys. Stat. Sol. (c) **8**, 2170 (2011).
[71] L. Lu, Y. H. Zhu, Z. T. Chen, and T. Egawa, J. Appl. Phys. **109**, 113537 (2011).
[72] A. Armstrong, T. A. Henry, D. D. Koleske, M. H. Crawford, K. R. Westlake, and S. R. Lee, Appl. Phys. Lett. **101**, 162102 (2012).
[73] L. C. Le, D. G. Zhao, D. S. Jiang, L. Li, L. L. Wu, P. Chen, Z. S. Liu, Z. C. Li, Y. M. Fan, J. J. Zhu, H. Wang, S. M. Zhang, and H. Yang, Appl. Phys. Lett. **101**, 252110 (2012).
[74] S.-K. Lee, H. S. Lim, J.-H. Lee, H.-S. Kwack, H. K. Cho, H.-K. Kwon, and M. S. Oh, J. Appl. Phys. **111**, 103115 (2012).
[75] D.-Y. Lee, S.-H. Han, D. J. Lee, J. W. Lee, D.-J. Kim, Y. S. Kim, S.-T. Kim, and J.-Y. Leem, Appl. Phys. Lett. **102**, 011115 (2013).
[76] N. A. Modine, A. M. Armstrong, M. H. Crawford, and W. W. Chow, J. Appl. Phys. **114**, 144502 (2013).
[77] R. Vaxenburg, E. Lifshitz, and A. L. Efros, Appl. Phys. Lett. **102**, 031120 (2013).
[78] Y. C. Shen, G. O. Mueller, S. Watanabe, N. F. Gardner, A. Munkholm, and M. R. Krames, Appl. Phys. Lett. **91**, 141101 (2007).
[79] A. David and M. J. Grundmann, Appl. Phys. Lett. **97**, 033501 (2010).
[80] C. Netzel, S. Hatami, V. Hoffmann, T. Wernicke, A. Knauer, M. Kneissl, and M. Weyers, Phys. Stat. Sol. (c) **8**, 2151 (2011).
[81] Y. Dong, J.-H. Song, H.-J. Kim, T.-S. Kim, B.-J. Ahn, J.-H. Song, I.-S. Cho, W.-T. Im, Y. Moon, S.-M. Hwang, S.-K. Hong, and S.-W. Lee, J. Appl. Phys. **109**, 043103 (2011).
[82] C. Lu, L. Wang, J. Lu, R. Li, L. Liu, D. Li, N. Liu, L. Li, W. Cao, W. Yang, W. Chen, W. Du, C.-T. Lee, and X. Hu, J. Appl. Phys. **113**, 013102 (2013).
[83] J. Hader, J. V. Moloney, S. W. Koch, and W. W. Chow, IEEE J. Select. Topics Quantum Electron. **9**, 688 (2003).
[84] M. Gladysiewicz, R. Kudrawiec, M. Syperek, J. Misiewicz, M. Siekacz, G. Cywinski, C. Skierbiszewski, and T. Suski, Phys. Stat. Sol. (c) **8**, 2273 (2011).
[85] M. Gladysiewicz, R. Kudrawiec, J. Misiewicz, M. Siekacz, G. Cywinski, and C. Skierbiszewski, Phys. Stat. Sol. (c) **8**, 2282 (2011).
[86] H. Haug and S. W. Koch, Phys. Rev. A **39**, 1887 (1989).
[87] W. W. Chow, A. Knorr, and S. W. Koch, Appl. Phys. Lett. **67**, 754 (1995).
[88] A. Girndt, F. Jahnke, S. W. Koch, and W. W. Chow, Mater. Sci. Eng. B **50**, 174 (1997).
[89] W. W. Chow and S. W. Koch, *Semiconductor-Laser Fundamentals. Physics of the Gain Materials* (Springer-Verlag, Berlin, 1999).
[90] S.-H. Park, D. Ahn, and J.-W. Kim, Appl. Phys. Lett. **94**, 041109 (2009).
[91] S.-H. Park, Y.-T. Moon, J. S. Lee, H. K. Kwon, J. S. Park, and D. Ahn, Phys. Stat. Sol. (a) **208**, 195 (2011).

[92] J. Hader, J. V. Moloney, and S. W. Koch, in *SPIE Photonics West, Gallium Nitride Materials and Devices VIII*, Vol. 8625, Proceedings of the SPIE (San Francisco, CA, 2013) pp. 86251M–86251M–10.
[93] M. Farahmand, C. Garetto, E. Bellotti, K. F. Brennan, M. Goano, E. Ghillino, G. Ghione, J. D. Albrecht, and P. P. Ruden, IEEE Trans. Electron Devices **ED-48**, 535 (2001).
[94] E. Bellotti, F. Bertazzi, and M. Goano, J. Appl. Phys. **101**, 123706 (2007).
[95] F. Bertazzi, M. Moresco, and E. Bellotti, J. Appl. Phys. **106**, 063718 (2009).
[96] E. Bellotti, F. Bertazzi, S. Shishehchi, M. Matsubara, and M. Goano, IEEE Trans. Electron Devices **60**, 3204 (2013).
[97] V. O. Turin, Solid-State Electron. **49**, 1678 (2005).
[98] E. M. Azoff, IEEE Trans. Electron Devices **36**, 609 (1989).
[99] Z.-M. S. Li, Y.-Y. Li, and G.-P. Ru, J. Appl. Phys. **110**, 093109 (2011).
[100] M. Grupen and K. Hess, IEEE J. Quantum Electron. **34**, 120 (1998).
[101] M. E. Vallone, J. Appl. Phys. **114**, 053704 (2013).
[102] C. S. Xia, S. Li, Y. Sheng, L. W. Cheng, W. D. Hu, and W. Lu, in *12th International Conference on Numerical Simulation of Optoelectronic Devices (NUSOD 2012)* (Shanghai, China, 2012) pp. 21–22.
[103] C. S. Xia, Z. M. S. Li, Z. Q. Li, Y. Sheng, Z. H. Zhang, W. Lu, and L. W. Cheng, Appl. Phys. Lett. **100**, 263504 (2012).
[104] P. Rinke, M. Winkelnkemper, A. Qteish, D. Bimberg, J. Neugebauer, and M. Scheffler, Phys. Rev. B **77**, 075202 (2008).
[105] M. Suzuki, T. Uenoyama, and A. Yanase, Phys. Rev. B **52**, 8132 (1995).
[106] I. Vurgaftman and J. R. Meyer, J. Appl. Phys. **94**, 3675 (2003).
[107] K. A. Bulashevich and S. Y. Karpov, Phys. Stat. Sol. (c) **5**, 2066 (2008).
[108] B. Galler, P. Drechsel, R. Monnard, P. Rode, P. Stauss, S. Froehlich, W. Bergbauer, M. Binder, M. Sabathil, B. Hahn, and J. Wagner, Appl. Phys. Lett. **101**, 131111 (2012).
[109] A. Hangleiter, Phys. Rev. B **48**, 9146 (1993).
[110] E. Kioupakis, Q. Yan, and C. G. Van de Walle, Appl. Phys. Lett. **101**, 231107 (2012).
[111] J. Hader, J. V. Moloney, B. Pasenow, S. W. Koch, M. Sabathil, N. Linder, and S. Lutgen, Appl. Phys. Lett. **92**, 261103 (2008).
[112] R. Vaxenburg, A. Rodina, E. Lifshitz, and A. L. Efros, Appl. Phys. Lett. **103**, 221111 (2013).
[113] D. Watson-Parris, M. J. Godfrey, P. Dawson, R. A. Oliver, M. J. Galtrey, M. J. Kappers, and C. J. Humphreys, Phys. Rev. B **83**, 115321 (2011).
[114] S. Hammersley, T. J. Badcock, D. Watson-Parris, M. J. Godfrey, P. Dawson, M. J. Kappers, and C. J. Humphreys, Phys. Stat. Sol. (c) **8**, 2194 (2011).
[115] Y.-R. Wu, R. Shivaraman, K.-C. Wang, and J. S. Speck, Appl. Phys. Lett. **101**, 083505 (2012).
[116] Y.-R. Wu, S. ting Yeh, D.-W. Lin, C. kang Li, H.-C. Kuo, and J. S. Speck, in *13th International Conference on Numerical Simulation of Optoelectronic Devices (NUSOD 2013)* (Vancouver, 2013) pp. 111–112.
[117] R. Sarkissian, S. T. Roberts, T.-W. Yeh, S. Das, S. E. Bradforth, J. O'Brien, and P. D. Dapkus, Appl. Phys. Lett. **103**, 041123 (2013).
[118] F. Bertazzi, M. Goano, and E. Bellotti, in *SPIE Photonics West, Physics and Simulation of Optoelectronic Devices XXI*, Vol. 8619, Proceedings of the SPIE (San Francisco, CA, 2013) pp. 86191G–1–86191G–9.
[119] F. Bertazzi, X. Zhou, M. Goano, E. Bellotti, and G. Ghione, "Full-band electronic structure calculation of semiconductor nanostructures: a reduced-order approach," arXiv:1304.1019 (2013).
[120] D. Jena, J. Simon, A. K. Wang, Y. Cao, K. Goodman, J. Verma, S. Ganguly, G. Li, K. Karda, V. Protasenko, C. Lian, T. Kosel, P. Fay, and H. Xing, Phys. Stat. Sol. (a) **208**, 1511 (2011).
[121] J. Pal, M. A. Migliorato, C.-K. Li, Y.-R. Wu, B. G. Crutchley, I. P. Marko, and S. J. Sweeney, J. Appl. Phys. **114**, 073104 (2013).
[122] W. W. Chow, M. H. Crawford, J. Y. Tsao, and M. Kneissl, Appl. Phys. Lett. **97**, 121105 (2010).
[123] I.-L. Lu, Y.-R. Wu, and J. Singh, Phys. Stat. Sol. (c) **8**, 2393 (2011).
[124] J. Iveland, L. Martinelli, J. Peretti, J. S. Speck, and C. Weisbuch, Phys. Rev. Lett. **110**, 177406 (2013).
[125] F. Bertazzi, M. Goano, X. Zhou, M. Calciati, G. Ghione, M. Matsubara, and E. Bellotti, "Comment on "Direct measurement of Auger electrons emitted from a semiconductor light-emitting diode under electrical injection: Identification of the dominant mechanism for efficiency droop" [Phys. Rev. Lett. 110, 177406 (2013)]," arXiv:1305.2512 (2013).
[126] J. Wu, J. Appl. Phys. **106**, 011101 (2009).
[127] S. Chiaria, M. Goano, and E. Bellotti, IEEE J. Quantum Electron. **47**, 661 (2011).